



## **Early Holocene Thermal Maximum recorded by branched tetraethers and pollen in Western Europe (Massif Central, France)**

Céline Martin, Guillemette Menot, Nicolas Thouveny, Odile Peyron, Valérie Andrieu-Ponel, Vincent Montade, Nina Davtian, Maurice Reille, Edouard Bard

### **► To cite this version:**

Céline Martin, Guillemette Menot, Nicolas Thouveny, Odile Peyron, Valérie Andrieu-Ponel, et al.. Early Holocene Thermal Maximum recorded by branched tetraethers and pollen in Western Europe (Massif Central, France). *Quaternary Science Reviews*, 2020, 228, pp.106109. <10.1016/j.quascirev.2019.106109>. <hal-02415846>

**HAL Id: hal-02415846**

**<https://amu.hal.science/hal-02415846v1>**

Submitted on 17 Dec 2019

**HAL** is a multi-disciplinary open access archive for the deposit and dissemination of scientific research documents, whether they are published or not. The documents may come from teaching and research institutions in France or abroad, or from public or private research centers.

L'archive ouverte pluridisciplinaire **HAL**, est destinée au dépôt et à la diffusion de documents scientifiques de niveau recherche, publiés ou non, émanant des établissements d'enseignement et de recherche français ou étrangers, des laboratoires publics ou privés.



Distributed under a Creative Commons CC BY-NC-ND 4.0 - Attribution - Non-commercial use - No Derivative Works - International License

# Early Holocene Thermal Maximum recorded by branched tetraethers and pollen in Western Europe (Massif Central, France)

Céline Martin <sup>a, b</sup>, Guillemette Ménot <sup>b, \*</sup>, Nicolas Thouveny <sup>a</sup>, Odile Peyron <sup>c</sup>,  
Valérie Andrieu-Ponel <sup>d</sup>, Vincent Montade <sup>c, e</sup>, Nina Davtian <sup>a</sup>, Maurice Reille <sup>f</sup>,  
Edouard Bard <sup>a</sup>

<sup>a</sup> Aix Marseille Univ, CNRS, IRD, INRA, Coll France, CEREGE, Europôle Méditerranéen de l'Arbois BP 80 13545 Aix-en-Provence cedex 4, France

<sup>b</sup> Univ Lyon, ENS de Lyon, Université Lyon 1, CNRS, UMR 5276 LGL-TPE, F-69364, Lyon, France

<sup>c</sup> Institut des Sciences de l'Evolution de Montpellier, Univ. of Montpellier, CNRS, IRD, EPHE, Montpellier, France

<sup>d</sup> Aix Marseille Univ, Univ Avignon, CNRS, IRD, IMBE, Europôle Méditerranéen de l'Arbois, BP 80 13545 Aix-en-Provence cedex 4, France

<sup>e</sup> Dept. of Palynology and Climate Dynamics, Albrecht-von-Haller-Institute for Plant Sciences, Georg-August-University of Göttingen, Untere Karspüle 2, 37073 Göttingen, Germany

<sup>f</sup> Venède, 48000 Mende, France

## ARTICLE INFO

### Article history:

Received 3 September 2019

Received in revised form

25 November 2019

Accepted 25 November 2019

Available online xxx

### Keywords:

Holocene

Quantitative paleoclimate reconstructions

Continental biomarkers

Branched GDGTs

Pollen

Transfer functions

Western Europe

## ABSTRACT

The evolution of temperatures during the Holocene is controversial, especially for the early Holocene. The occurrence of the Holocene Thermal Maximum (HTM) during the early Holocene has recently been reconsidered and seasonal biases have been suggested in the paleoclimatic proxies. High regional variability and a low number of reliable and continuous quantitative reconstructions compared with the oceanic realm further complicate study of the Holocene climate in the continental realm. We analyzed branched glycerol dialkyl glycerol tetraethers (brGDGTs), an organic paleothermometer, and palynological signals as part of a multiproxy analysis of the sedimentary record from Lake St Front, in the Massif Central (France). Identification of a shift in brGDGT sources through the Holocene required removing terrigenous influences from the temperature signal. BrGDGT- and pollen-inferred paleotemperature reconstructions (based on the Modern Analog Technique and the Weighted Averaging Partial Least Squares method) were compared. Both showed a thermal maximum during the early Holocene followed by a decrease of temperatures. We evaluated biases which could potentially influence the reconstructed signal. There was no evidence for a summer temperature bias either for brGDGT-derived temperatures or for pollen-derived temperatures. The Lake St Front data, in agreement with other regional records, confirm the occurrence of the HTM as a general warm period during the early Holocene followed by mid-Holocene cooling in Western Europe and suggest that seasonal biases are not the main explanation of the Holocene conundrum — the disagreement between model simulations and proxy-based temperature reconstructions for the northern hemisphere.

## 1. Introduction

The current interglacial, the Holocene, starting about 11.7 kyr BP, is a period of relative climatic stability compared to the large-scale climate variability occurring during glacial-interglacial transitions (e.g., Mayewski et al., 2004; Rasmussen et al., 2014; Rehfeld et al., 2018). Nonetheless, paleoclimatic reconstructions obtained from

various proxies reveal significant changes in temperature and/or moisture balance over the entire period at millennial and centennial scales (e.g., Bond et al., 2001; Davis et al., 2003; Roberts et al., 2011; Wanner et al., 2011; Magny et al., 2013). Many studies suggest the occurrence, in the northern hemisphere, of an early Holocene warm period between ~10 and 6 kyr cal BP: the Holocene Thermal Maximum (HTM). This HTM was followed by a global cooling trend during the mid and late Holocene (e.g., Mann et al., 2009; Renssen et al., 2012; Marcott et al., 2013; PAGES 2k Consortium et al., 2013; Wanner et al., 2015). However, this trend contradicts the expected and simulated warming trend caused by the retreat of the large

\* Corresponding author.

E-mail addresses: [celine.martin24@lilo.org](mailto:celine.martin24@lilo.org) (C. Martin), [guillemette.menot@ens-lyon.fr](mailto:guillemette.menot@ens-lyon.fr) (G. Ménot).

glacial ice sheets in North America and Eurasia (e.g., Liu et al., 2014; Zhang et al., 2018). This retreat continued for several millennia after the Younger Dryas/Holocene transition (Peltier, 2004) and was associated with albedo modifications and a rise in atmospheric greenhouse gases (e.g., Liu et al., 2014). Marsicek et al. (2018) proposed a pollen-based paleoclimate reconstruction for North America and Europe based on numerous records. In this reconstruction, the summer temperature presented an early HTM and a subsequent decrease in response to summer insolation fluctuations, while the mean annual temperatures show a continuous warming trend until 2 kyr cal BP. In this study, the HTM appears to reflect a bias towards a summer signal. Qualitative temperature records from Eurasia (Baker et al., 2017) and quantitative temperature reconstructions from Eastern Russia (Meyer et al., 2017) support the warming trend through the Holocene evidenced by Marsicek et al. (2018). Several discrepancies between proxy-inferred climate reconstructions and model outputs persist and suggest: i) large regional heterogeneities (Davis et al., 2003; Kaufman et al., 2004; Jansen et al., 2007, 2008; Renssen et al., 2012; Peyron et al., 2017; Marsicek et al., 2018); ii) different trends depending on the season considered (Mauri et al., 2014, 2015; Rehfeld et al., 2016; Marsicek et al., 2018); iii) seasonal biases in proxies (Marcott et al., 2013; Liu et al., 2014; Rehfeld et al., 2016; Samartin et al., 2017; Marsicek et al., 2018; Hou et al., 2019); iv) under-estimation of some forcing factors by models (mineral dust, Liu et al., 2018, or deglaciation, Renssen et al., 2009), and v) biases in the climate sensitivity of current climate models (Liu et al., 2014; Mauri et al., 2014; Zhang et al., 2018). Therefore, climate changes during the Holocene at local, regional and global scales remain an area of active research and debate. This suggests a need for development of new quantitative climate proxies and multiproxy approaches that can help identify the potential biases of currently used proxies and improve the reliability of each proxy-inferred climate record.

At a millennial scale, prominent climate events and secular climatic oscillations have been identified in the northern hemisphere (e.g., Alley et al., 1997; Magny, 2004; Mayewski et al., 2004; Fleitmann et al., 2008; Combourieu-Nebout et al., 2013; Peyron et al., 2013) and correlated to the Bond events in the North Atlantic (Bond et al., 2001). Continental archives generally offer better resolution than oceanic records allowing for the resolution of secular time scales and reflecting the spatial heterogeneity of climatic and environmental changes. Continental archives are, however, rarely continuous over long time periods (Alley et al., 1997; Hoek and Bos, 2007; Fleitmann et al., 2008). Only a few long and continuous quantitative reconstitutions of climatic parameters (such as temperature or precipitation) are available for Western Europe (e.g., Moreno et al., 2014). Therefore, the continental response to these abrupt climatic events needs to be clarified.

Branched glycerol dialkyl glycerol tetraethers (brGDGTs) have provided new perspectives on continental temperature reconstructions. These ubiquitous membrane-spanning lipids are of bacterial origin and their producers are mostly unknown except for subdivisions of *Acidobacteria* (Weijers et al., 2006a, 2009; Sinninghe Damsté et al., 2011, 2014, 2018). They have been identified in a wide range of environments like soils, paleosoils, loess, coastal marine and lake sediments (e.g., Schouten et al., 2000; Hopmans et al., 2004; Weijers et al., 2006a, 2007a, 2007b; Sinninghe Damsté et al., 2008; Huguet et al., 2010; Loomis et al., 2011). Branched GDGTs from terrigenous sources are transported, via soil erosion and runoff, to aquatic systems and accumulate in the sediments where they can be preserved (e.g., Hopmans et al., 2004). The signal recorded in lake sediments thus reflects the conditions of the catchment basin and its changes. BrGDGTs have a wide diversity of structures allowing brGDGTs producers to modify the composition of their cellular

membrane lipids to adapt their functionality to specific environmental parameters (e.g., Weijers et al., 2007b). Based on the relative distribution of the distinct forms of brGDGTs in soils, indices have been defined. The Cyclization ratio of Branched Tetraethers (CBT) is related to soil pH and the Methylation index of Branched Tetraethers (MBT) is related to the Mean Annual Air Temperature (MAAT) and soil pH (Weijers et al., 2007b; Peterse et al., 2012). The MBT/CBT-proxy is increasingly used to reconstruct past temperatures as a quantitative paleothermometer (e.g., Niemann et al., 2012; Sanchi et al., 2014; Watson et al., 2018). The first global calibration was established by Weijers et al. (2007b). Since then, numerous calibrations have been developed. De Jonge et al. (2013, 2014) improved the chromatography techniques, allowing separation of the 5-, 6- and 7-methyl isomers of hexa- and pentamethylated brGDGTs (Ding et al., 2016). They defined new indices and established new calibrations. Lake sediment studies have involved the development of specific calibrations (Bendle et al., 2010; Blaga et al., 2010; Tierney et al., 2010; Sun et al., 2011; Zink et al., 2016; Russell et al., 2018). Most of these studies demonstrated that in situ production in the water column or in the sediment could occur, potentially biasing the results obtained (Tierney and Russell, 2009; Loomis et al., 2011; Tierney et al., 2012; Wang et al., 2012a; Buckles et al., 2014a, 2014b). However, soil organic matter inputs can be tracked and potentially corrected (Hopmans et al., 2004; Sinninghe Damsté, 2016; Xiao et al., 2016).

Pollen data are often used as a proxy to quantitatively reconstruct climate changes, especially during the Holocene (e.g., Peyron et al., 2011, 2013, 2017; Mauri et al., 2014; Guiot and Kaniewski, 2015; Tarroso et al., 2016; Bini et al., 2019). Modern pollen data are related to their present climatic parameters, and the derived relationship is applied to the fossil pollen samples. Several methods exist for quantitatively reconstructing past climates from pollen data. Assemblage approaches, such as Modern Analog Technique (MAT; Overpeck et al., 1985; Guiot, 1990) are based on similarity calculation and consist of selecting a set of modern pollen assemblages that most closely resembles each of the fossil pollen assemblages. Mathematical transfer functions such as the Weighted Averaging Partial Least Squares method (WAPLS) developed by ter Braak and Juggins (1993) are based on statistical calibration. However, new methods based on pollen data and vegetation modelling have also been recently developed and allow consideration of the direct effect of CO<sub>2</sub> on vegetation and climate changes (Guiot and Kaniewski, 2015; Wei et al., 2019). Reconstructions of temperature variations in Europe during the Holocene derived from brGDGTs are uncommon and comparison between pollen- and brGDGT-inferred temperatures are rare (Holtvoeth et al., 2017; Miller et al., 2018; Watson et al., 2018).

In this study, we considered the Lake St Front, a maar lake located 1230 m above sea level in the eastern Velay region (Massif Central, France), at the convergence of Atlantic and Mediterranean climatic influences. This lake provided one of the key paleoclimatic records for Western Europe covering the entire last glacial/interglacial cycle and the end of the Marine Isotope Stage (MIS) 6 (Vlag et al., 1997). The Massif Central has been widely explored for palynological studies and has provided key long sequences such as the lac du Bouchet, which covers the last four climate cycles (e.g., de Beaulieu et al., 1984, 1988; Reille and de Beaulieu, 1988, 1990; de Beaulieu and Reille, 1992; Reille et al., 1992). In the Massif Central, the environmental changes that occurred during the late-glacial and early Holocene have been particularly well documented by multi-proxy approaches (e.g., Gandouin et al., 2016; Ponel et al., 2016).

Here, we introduce a well-dated Holocene pollen record and two new Holocene paleotemperature reconstructions based on pollen assemblages and brGDGTs from Lake St Front. In a previous study, we compared the brGDGT distributions of catchment and top

sediment samples and concluded that the brGDGTs present in lake sediments originated from both soils and in situ production in the lake (Martin et al., 2019). The  $\Sigma\text{IIIa}/\Sigma\text{IIa}$  ratio (Xiao et al., 2016) appeared to be the only tool able to distinguish the source of brGDGTs in our setting and, when applied to the entire core, revealed a gradual change from aquatic to terrigenous source (Martin et al., 2019). These source changes precluded direct application of MBT/CBT calibrations and inference of past temperatures. In this study, based on the brGDGT analysis in Lake St Front, we established a binary mixing model to correct the signal from terrigenous inputs and infer the evolution of temperatures over the Holocene. We compared this record with the paleotemperatures derived from the pollen assemblages of the Lake St Front record using a multi-method approach (Modern Analog Technique and Weighted Averaging Partial Least Squares Regression) and discussed similarities and differences between the records. We then compared these new data to other regional and global temperature reconstructions in order to (1) evaluate potential biases, especially seasonal biases associated with the reconstructions based on brGDGTs and pollen; (2) determine if our records corroborate the occurrence of a Holocene Thermal Maximum in the Massif Central; (3) detect the local expression of abrupt climate changes identified on a hemispheric scale during the Holocene.

## 2. Material and methods

### 2.1. Lake St Front and modern climate setting

Lake St Front lies on the Meygal-Mézenc plateau in the eastern Velay in the Massif Central, France (44°58' lat N; 4°10' long E; 1234 m, Fig. 1A). The lake occupies a sub-circular crater (maar) cut through Quaternary basalts by a phreatomagmatic explosion (Mergoïl, 1987; Teulade et al., 1991). The lake diameter is 600 m and its maximum depth is 6 m (Fig. 1B). The lake catchment area is small (1.5 km<sup>2</sup>). The lake is supplied by rainfall and runoff and by aerial and sub-lacustrine springs connected to the local water table (Mergoïl et al., 1993). It is a eutrophic lake with a high potential for organic matter preservation. A small artificial outlet at the south-western shore of the lake constrains the present lake level. The surroundings are dominated by coniferous and deciduous forests (with *Pinus sylvestris* and *Quercus pubescens* dominant; Carles, 1956), grassland used as cattle pasture with numerous streams and a peat bog (Fig. 1B).

Modern climatic parameters were obtained from the instrumental database of Météo-France (<https://donneespubliques.meteofrance.fr>) at the nearby station of Mazet-Volamont (1130 m) located 11 km distant, for the period 2009–2017, and for longer data series, at the stations of Saint Julien Chapeuil (distance 9 km, altitude 810 m, period 1995–2017) and Le Puy en Velay (distance 22 km, altitude 833 m, period 1981–2010, Fig. 1C). Temperature values were corrected using a lapse rate of 0.6 °C/100 m. Mean annual temperatures vary between 6 and 9 °C with a mean value of 7 °C. Mean temperatures are 1 °C and 15 °C for winter and summer respectively, while daily maximum temperature can exceed 25 °C. The lake is generally frozen during at least three months each year (Fillod, 1985). The average annual amount of precipitation is about 1000 mm/year and the two wettest seasons are autumn and spring. Rainfalls are fed by humid air masses pushed by winds from the Atlantic Ocean and from the Mediterranean basin. Snowfalls are particularly important on the Eastern Velay plateau and occur on more than 50 days per year.

### 2.2. Sampling and core characteristics

Two coring campaigns were conducted in Lake St Front. In 1991,

three long piston core sequences, SFA (45 m), SFB (60 m) and SFC (22 m), were recovered in the central part of the lake (SF91 in Fig. 1B, Sup Table 2). In 2016, two new cores SF16-2 (19 m) and SF16-3 (13 m) were retrieved during a second campaign (SF16 in Fig. 1B, Sup Table 3). The water-sediment interface was also sampled with a 60 cm gravity core in the central part of the lake as well as at different locations near the shore (Fig. 1B, Table 1, Sup Table 3). Soils (2–5 cm depth), upper sediments of catchment streams (0–2 cm depth) and surface sediment in the shoreline were also sampled all around the lake (Fig. 1B, Table 1, Sup Table 3).

Correlations between all cores relied on low field magnetic susceptibility measured at 2 cm resolution using a Bartington susceptibility meter MS2 connected to a MS2C probe 90 mm diameter on the field. The magnetic susceptibility profiles allowed construction of a continuous composite sequence from SFB and SFC with SF16-2 and -3 filling the sedimentary hiatus identified in the 1991 cores corresponding to the late Glacial and the Holocene onset (Andrieu et al., 1995; Vlag et al., 1997). The present study focused on the upper 13 m of the composite sequence and the first 11.75 m of SFA. The Holocene part of the sequence is composed by organic “gyttjas”, an accumulation of vegetable fibers formed by autochthonous OM and soil degradation products packed in a relatively porous and gas rich clayey matrix (Rhoujjati, 1995).

The age model based on <sup>210</sup>Pb and <sup>30</sup><sup>14</sup>C measurements until 40.5 ka was previously discussed and published by Martin et al. (2019).

### 2.3. BrGDGT analysis

Branched GDGT analyses were carried out every 10 cm on samples stored frozen. Sediments were freeze-dried then powdered. Surface samples and soils were sieved prior to being powdered to remove macro-remains and roots. Total lipid extracts were obtained from 1 to 2 g of each sample using the accelerated solvent extraction method (ASE 350 Dionex system) with dichloromethane (DCM):methanol (MeOH) (9:1 v/v) at 120 °C and 80–100 bar. The lipids were then separated using Al<sub>2</sub>O<sub>3</sub> columns and hexane:DCM (1:1 v/v) to elute the apolar fraction, then MeOH:DCM (1:1 v/v) for the polar fraction (Sanchi et al., 2013). Analyses were performed on polar fractions with high-performance liquid chromatography/atmospheric pressure chemical ionization-mass spectrometry (HPLC/APCI-MS) using an Agilent 1260 Infinity HPLC coupled to an Agilent 6120 quadrupole mass spectrometer following the new method described in Hopmans et al. (2016) with the modifications of Davtian et al. (2018). The analyses were conducted at the CEREGE (Aix-en-Provence, France).

Each sample was run at least in duplicate. To determine the peak areas of each GDGT, we used the Agilent Chemstation chromatography management software which allows manual integration of the peak areas of [M + H]<sup>+</sup> ion traces of GDGTs (1292.3, 743.7, 1050.0, 1048.0, 1046.0, 1036.0, 1034.0, 1032.0, 1022.0, 1020.0, 1018.0 according to Davtian et al., 2018; Sup Tables 2 and 3). The relative response factor (RRF; Huguet et al., 2006) was inferred by running mixed samples of C46 and GDGT-0 (caldarchaeol, 1:1). A sample of surface sediments from Lake St Front was used as an external standard and run at the beginning and the end of each batch to test the process reproducibility and to detect instrument drift.

For all of the statistical tests we used PAST software (ver. 3.04; Hammer et al., 2001).

### 2.4. Calculation of brGDGT-based indices

The  $\Sigma\text{IIIa}/\Sigma\text{IIa}$  ratio was determined to identify brGDGT sources following Xiao et al. (2016) with the modifications of Martin et al. (2019):



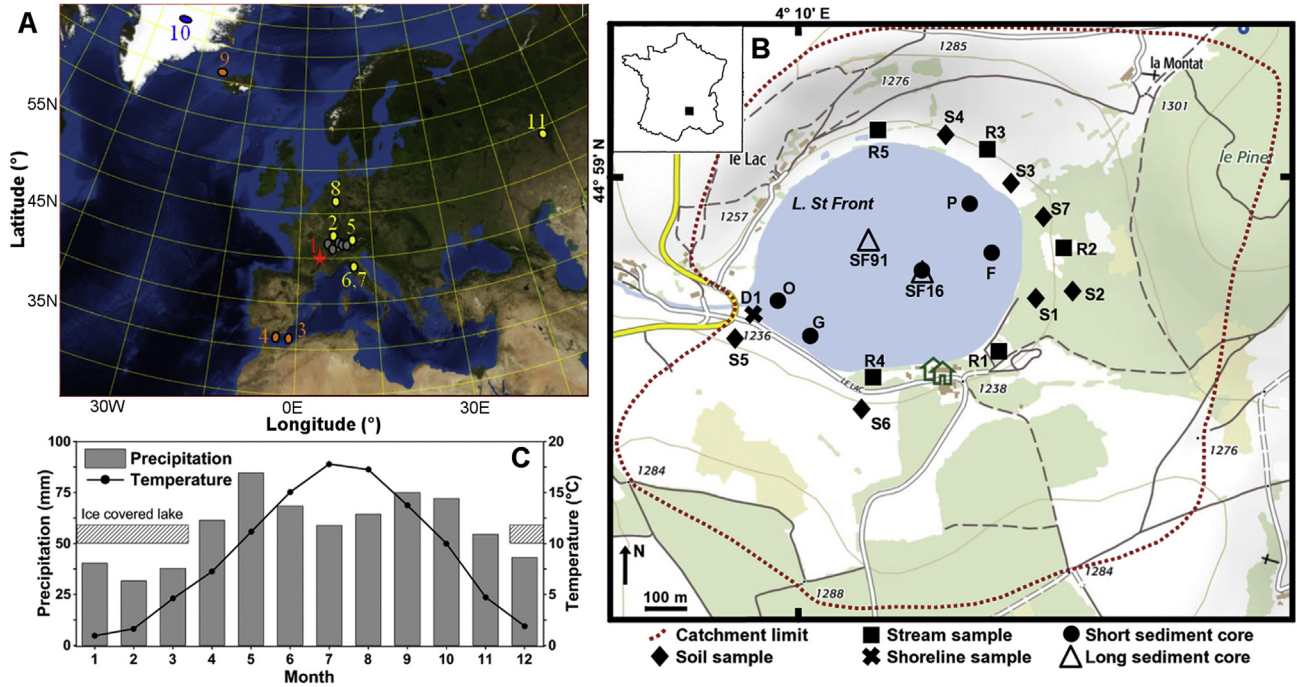


**Fig. 1. Locations of Lake St Front and records of interest.** **A.** Location of the records discussed in the text, (1) Lake St Front (red star, this study), (2) Milandre Cave, (3) Mediterranean sites MD95-2043 and (4) ODP161-976, (5) Schwarzsee ob Sölden, (6) Lake Gemini, (7) Lake Verdarolo, (8) Bunker Cave, (9) North Atlantic site MD99-2266, (10) Greenland Ice Sheet Project 2 (GISP2) and (11) Kinderlinskaya Cave. The grey points represent the lakes Hinterburgsee, Stazersee, Foppe, Maloja Riegel, Lautrey and Anterne used by Heiri et al. (2015) to build a temperature synthesis. See Sup Table 1 for more information. **B.** Map of Lake St Front and sampling locations of the long sediment cores (open triangles), short interface top sediment cores (circles), shoreline sediments (crosses) and catchment samples, soils (diamonds) and streams (squares), associated with their reference name. The limits of the catchment area are marked by the dotted red line and the woodland area are colored in green. Topographic map modified from the Institut national de l'information géographique et forestière (IGN). The insert shows a map of France with the localization of the lake. Modified from Martin et al. (2019). **C.** Monthly variations of precipitation amount (bars) and mean temperature (line with circles) for Le Puy en Velay Meteorological Station (22 km from Lake St Front to the northwest, 833 m) over the period of 1981–2010 (data from Météo-France database <https://donneespubliques.meteofrance.fr/>). The period of ice cover of Lake St Front is represented by a hatched rectangle. (For interpretation of the references to color in this figure legend, the reader is referred to the Web version of this article.)

$$\frac{\Sigma IIIa}{\Sigma IIa} = \frac{IIIa + IIIa' + IIIa'' + IIIa_7}{IIa + IIa' + IIa_7} \quad (1)$$

The definitions of Weijers et al. (2007b), Peterse et al. (2012) and De Jonge et al. (2014) were used to calculate MBT, MBT', MBT'<sub>5Me</sub> and CBT indices with the modification of De Jonge et al. (2014) including the 6-methyl (6-Me) forms denoted as X'. We included the 7-methyl (7-Me) forms found by Ding et al. (2016) represented as X<sub>7</sub>:

$$MBT = Ia + Ib + Ic / \Sigma brGDGTs \quad (2)$$

$$MBT' = \frac{Ia + Ib + Ic}{Ia + Ib + Ic + IIa + IIa' + IIa_7 + IIb + IIb' + IIc + IIc' + IIIa + IIIa' + IIIa'' + IIIa_7} \quad (3)$$

$$MBT'_{5Me} = \frac{Ia + Ib + Ic}{Ia + Ib + Ic + IIa + IIb + IIc + IIIa} \quad (4)$$

$$CBT = -\log(IIb + IIb' / Ia + IIa + IIa' + IIa_7) \quad (5)$$

To calculate the mean annual air temperature (MAAT), we tested the lacustrine calibration of Sun et al. (2011):

$$MAAT = 3.949 - 5.593 \times CBT + 38.213 \times MBT \quad n = 100, R^2 = 0.73, RMSE = 4.27^\circ C \quad (6)$$

the soil calibration of Peterse et al. (2012):

$$MAAT = 0.81 - 5.67 \times CBT + 31 \times MBT' \quad n = 176, R^2 = 0.59, RMSE = 5^\circ C \quad (7)$$

and the lacustrine calibration of Russell et al. (2018):

$$MAAT = -1.21 + 32.42 \times MBT'_{5Me} \quad n = 65, R^2 = 0.92, RMSE = 2.44^\circ C \quad (8)$$

The analytical reproducibility was obtained by running an external standard several times ( $n=16$ ). The values were 0.003 for the MBT and MBT' indices, 0.006 for the MBT'<sub>5Me</sub> index, 0.01 for the CBT index and 0.2 °C for MAAT calculated with the Sun et al. (2011)

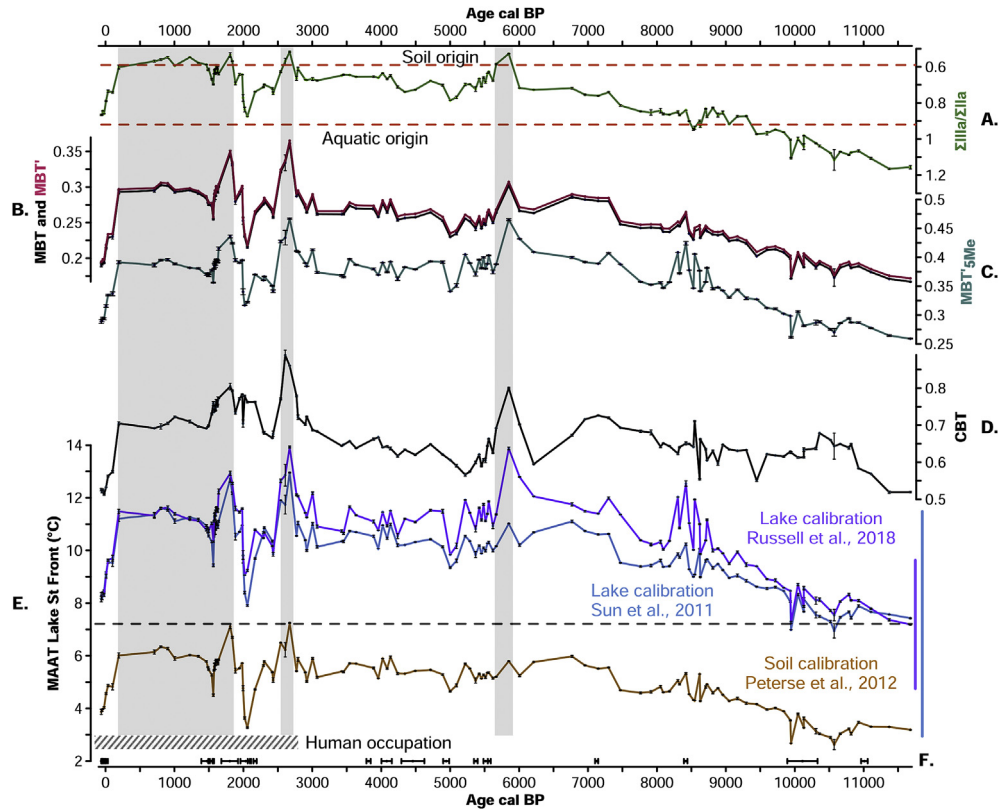


**Fig. 2.** BrGDGT proxies and associated temperature reconstructions in Lake St Front through the Holocene. **A.**  $\Sigma\text{IIIa}/\Sigma\text{IIa}$  ratio (Martin et al., 2019) with the upper limit of soil realm and the lower limit of aquatic realm (Xiao et al., 2016, dashed lines). Note that the axis has been reversed. **B.** MBT (black line), MBT' (pink line). **C.** MBT'<sub>5Me</sub> (blue-green line) and **D.** CBT with their analytical errors ( $1\sigma$  values). **E.** Mean annual air temperatures (MAAT) reconstructed with Sun et al. (2011, blue curve), Russell et al. (2018, purple curve) and Peterse et al. (2012, brown curve) calibrations compared with the present mean annual temperature at St Front (black dashed line). The vertical bars represent the error associated with Sun et al. (2011) and Russell et al. (2018) calibrations (blue and purple lines, respectively). **F.**  $^{14}\text{C}$  calibrated ages and  $^{210}\text{Pb}$  dates (Martin et al., 2019). Shaded rectangles highlight the periods when  $\Sigma\text{IIIa}/\Sigma\text{IIa}$  values are below soil origin higher limit. The period of permanent human occupation is marked by a hatched rectangle. (For interpretation of the references to color in this figure legend, the reader is referred to the Web version of this article.)

and Russell et al. (2018) calibrations, and  $0.1^\circ\text{C}$  for MAAT calculated with the Peterse et al. (2012) calibration.

## 2.5. Pollen-inferred temperature reconstructions

We used here the pollen analyses conducted on 106 samples from the SFA profile (Martin et al., 2019 and Fig. 3, Sup Table 4) to provide the St Front climate reconstruction. A multi-method has been adopted to improve the reliability of the temperature reconstructions (Peyron et al., 2013).

### 2.5.1. Method 1: Modern Analog Technique

Pollen-inferred temperature reconstructions were conducted using the Modern Analog Technique (MAT) (Guiot, 1990). This is an assemblage approach, which consists of selecting the set of modern pollen assemblages that most closely resembles each fossil pollen assemblage. Comparing them in terms of taxa composition and abundance assesses the resemblance between modern and fossil pollen assemblages. Their (dis)similarity is quantified using squared-chord distances in order to reduce the influence of the few relatively abundant taxa in the samples. Once a set of modern samples has been selected as analogs, climatic parameters are attributed to each fossil sample as the weighted average of the modern samples climate. The weights used are the inverse of the chord distance, which allows the most similar analogs to have the greater influence on the climate estimates obtained. The number of analogs chosen in this study was 8, using a leave-one-out cross-

validation test. The method is based on a large data set of modern pollen samples (3190), mostly located in Europe, Siberia and the Mediterranean region (Peyron et al., 2017). We used here the basic Modern Analog Technique, i.e. without a plant functional type (PFTs) transformation (Mauri et al., 2015) and without the application of constraints such as lake-levels or biome for the analogs selection (Guiot et al., 1993). The plant functional type transformation is strongly dependent on the accuracy of the PFTs-taxa assignment and the biome constraint is mainly used to distinguish cold and warm steppe vegetation which was not relevant to this study.

### 2.5.2. Method 2: Weighted averaging partial least squares method

In contrast to the MAT based on a comparison of past assemblages to modern pollen assemblages, the Weighted Averaging Partial Least Squares (WAPLS) developed by ter Braak and Juggins (1993) requires a statistical calibration. The WAPLS is a transfer function which assumes that the relationship between pollen percentages and climate is unimodal. The modern pollen data set (the same as with the MAT: 3190 modern pollen assemblages) is considered as a large matrix with  $n$  dimensions, corresponding to each of the pollen taxa within the data set. WAPLS operates by compressing the overall data structure into latent variables. Several taxa are directly related to the climate parameters of interest. To avoid co-linearity among the taxa, the matrix is reduced to a smaller number of components based on both linear predictors of the parameter of interest and the residual structure of the data

**Table 1**

Results of the different calibrations on the catchment samples and top sediments of Lake St Front.  $n=18$  for catchment samples and  $n=7$  for core-tops.

Sample name	Sample provenance	MAAT Sun et al. (2011)	MAAT Loomis et al. (2012)	MAAT Russell et al. (2018)	Tgrowth Dang et al. (2018)	MAAT MBT <sub>5Me</sub> De Jonge et al. (2014)	MAAT T <sub>mr</sub> De Jonge et al. (2014)	MAAT Index 1 De Jonge et al. (2014)	MAAT Peterse et al. (2012)	MAAT <sub>mrsoil</sub> Naafs et al. (2017)
<b>Soils</b>										
S1	a Coniferous	11.4	13.8	12.5	14.4	5.4	4.7	2.4	4	2.4
	b forest	10.7	13.3	11.7	13.4	4.9	4	2	3.5	2
S2	a Deciduous	8.6	11.5	10.9	14.4	2.8	3.2	0.5	2.2	0.9
	b forest	10.3	13.2	12.8	16.3	4	5	2	3.6	2.5
S3	a Grassland,	11.6	13.6	10.9	11.1	6.1	3.2	3.3	3.6	2.7
	b peaty	12	13.6	11.9	13.1	6.1	4.1	2.7	3.4	2.7
S4	Peat bog	12.8	12.8	11.6	11.4	7.3	3.8	5.7	3.9	4
S5	Grassland	11.2	14	12.2	12.8	5.3	4.4	2.6	4.1	2.6
S6		12.2	14.1	13.3	12.5	6.3	5.5	4.1	5.1	3.7
S7	Marsh	13.3	15.8	12.2	11.8	7.5	4.5	4.9	4.4	4.2
<b>Streams</b>										
R1	a Grassland/	11.2	13	10.8	9.5	5.9	3	4.3	3.9	3.2
	b forest	10.6	12.2	10.3	8.7	5.4	2.6	4.2	3.7	3
R2	a Grassland/	11.8	13.7	11.8	10.6	6.2	4.1	4.5	4.3	3.8
	b forest	12.6	15	12.2	10.7	6.9	4.5	4.9	4.5	4.2
R3	a Grassland	11	11.1	11.1	9.2	5.8	3.4	5.3	4.3	3.7
	b	11.5	11.5	10.5	8.5	6.4	2.8	5.8	3.9	4
R4	Grassland/	11.3	11.8	11.5	9.4	5.9	3.8	4.8	4.3	3.7
	forest									
R5	Grassland/	12.9	11.1	11.8	12.7	7.3	4	4.1	3.9	3.4
	peat bog									
<b>Top sediments</b>										
D1	a Shoreline	7	8.6	8.8	5	2.2	1.1	2.8	3.4	2
	b	8.2	8.8	10.2	6.3	3.4	2.5	4.5	4.9	3.2
F	Near forest	7.6	7.5	8	4.9	3.2	0.4	4.5	3.9	3.1
P	Near peat	7.8	7.3	7.7	5	3.4	0.1	4.8	3.6	3.3
	bog shore									
O	Near outlet	7.5	6.9	7.5	4.9	3.1	-0.1	4.6	3.6	3.1
G	Near	7.9	8.4	9.1	6.9	3.5	1.4	4.8	4.7	3.4
	grassland									
	shore									
SF16-1A	Center of the lake	8.2	7.3	8.1	5.7	3.8	0.4	5	3.8	3.5

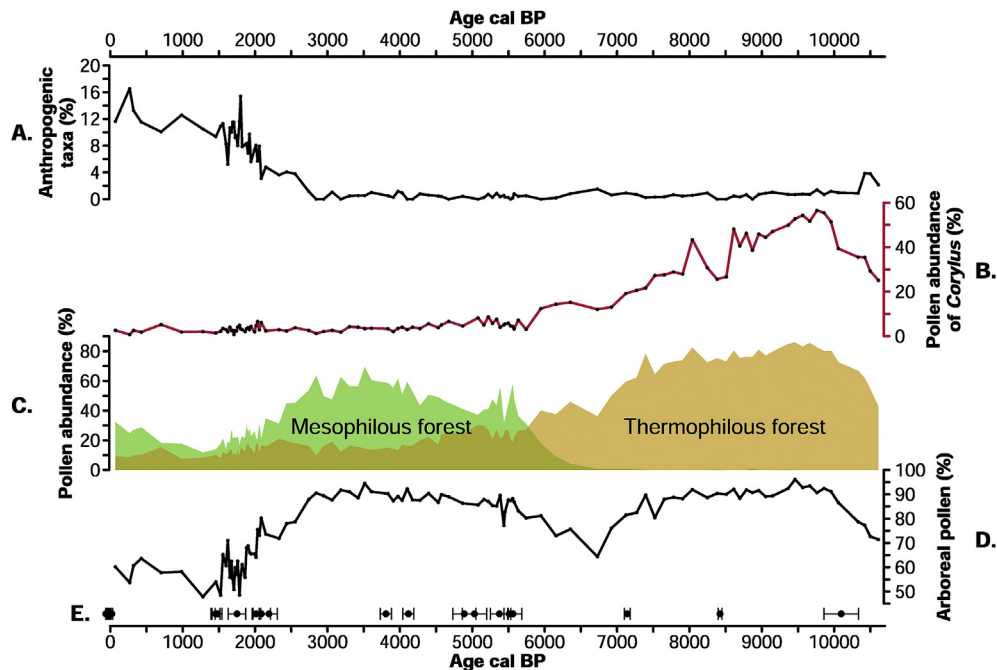


**Fig. 3. Selected taxa pollen percentages from Lake St Front sediments.** A. Percentages of pollen of anthropogenic taxa (*Plantago lanceolata*, *P. major*, *Rumex*, *Chenopodiaceae*, *Urtica*, *Cerealia*, *Secale* and *Juglans*, Martin et al., 2019). B. *Corylus* (pink curve) pollen percentages. C. Percentages of pollen from thermophilous (beige area, sum of *Acer*, *Corylus*, *Hedera*, *Ilex*, *Lonicera*, *Ostrya*, *Deciduous Quercus*, *Quercus ilex* t., *Pistacia*, *Sambucus*, *Sorbus*, *Tilia*, *Ulmus*, *Viburnum*, *Viscum*) and mesophilous (green area, sum of *Abies*, *Carpinus*, *Fagus*) tree pollen (Martin et al., 2019). D. Percentage of arboreal pollen (Martin et al., 2019). E.  $^{14}\text{C}$  calibrated ages and  $^{210}\text{Pb}$  dates (Martin et al., 2019). (For interpretation of the references to color in this figure legend, the reader is referred to the Web version of this article.)

when those predictors are removed. The modification of PLS proposed by [ter Braak and Juggins \(1993\)](#) requires transformation of the initial data set using weighted averaging along a gradient defined by the climate parameter of interest, such that the pollen taxa that best define the climate gradient are weighted more heavily than those that show little specificity to the gradient. Sample-specific errors have been calculated by bootstrapping, using the method described in [Birks et al. \(1990\)](#).

### 3. Results

#### 3.1. *BrGDGTs*

Through the Holocene, the  $\Sigma\text{IIIa}/\Sigma\text{IIa}$  ratio showed a general decreasing trend (from 1.2 to 0.6, [Fig. 2A](#), [Sup Table 5](#)) while the MBT, MBT', MBT'<sub>5Me</sub> and CBT indices increased through the Holocene (from 0.17 to 0.29, 0.17 to 0.3, 0.26 to 0.39 and 0.52 to 0.71 respectively, [Fig. 2B–D](#)). The reconstructed mean annual air temperatures (MAAT) followed the same increasing trend ([Fig. 2E](#)). Using the lacustrine calibrations the MAAT increased from 7.4 to 11.2 °C and from 7.2 to 11.5 °C with a maximal amplitude of 6 and 6.7 °C with the [Sun et al. \(2011\)](#) and [Russell et al. \(2018\)](#) calibrations, respectively ([Fig. 2E](#)). The soil calibration of [Peterse et al. \(2012\)](#) led to an increase from 3.2 to 6 °C with a maximal amplitude of 4.6 °C ([Fig. 2E](#)). The last 200 years display an opposite trend: the  $\Sigma\text{IIIa}/\Sigma\text{IIa}$  ratio increased by 0.26, the MBT, MBT' and MBT'<sub>5Me</sub> decreased by 0.1 and CBT by 0.2. MAAT decreased by 3.1 and 3.3 °C for the lake calibrations, [Sun et al. \(2011\)](#) and [Russell et al. \(2018\)](#), respectively, and 2.1 °C for the soil calibration ([Fig. 2](#)).

Rapid events interrupted these global trends particularly from 6 to 5.7, 2.7 to 2.5 and 2 to 0.2 kyr cal BP. During these events, the  $\Sigma\text{IIIa}/\Sigma\text{IIa}$  ratio dropped below 0.59, the limit for soil origin ([Fig. 2A](#); [Xiao et al., 2016](#)). These events coincided with the occurrence of MBT, MBT', MBT'<sub>5Me</sub> and CBT extreme values compared to nearby values (+0.05, +0.05, +0.05 and +0.1 on average respectively, [Fig. 2B–D](#)) which translated into peaks of reconstructed temperature (+1.2 °C, +1.5 °C and +0.9 °C respectively for the [Sun et al. \(2011\)](#) and [Russell et al. \(2018\)](#) lacustrine calibrations and the soil calibration, [Fig. 2E](#)).

BrGDGT-inferred mean annual temperature increased at the onset of the Holocene until 7 kyr cal BP for the [Sun et al. \(2011\)](#) lacustrine and soil calibrations (+3.7 °C and +2.8 °C, respectively) and until 5.9 kyr cal BP for the calibration of [Russell et al. \(2018\)](#), then remained relatively stable ([Fig. 2E](#)). However, several short-term cool episodes interrupted this trend around 9.2, 8.2, 5, 4 and 2 kyr cal BP.

#### 3.2. Pollen

##### 3.2.1. Modern Analog Technique

The MAT allowed reconstruction of a mean Holocene annual temperature of 8.3 °C which was 1.1 °C greater than the current value. The maximum of 11 °C and the minimum of 6.6 °C occurred at 10 and 1.5 kyr cal BP, respectively ([Fig. 4B](#)). Temperatures rapidly increased at the onset of the Holocene (+2.2 °C between 10.6 and 10 kyr cal BP, [Fig. 4B](#)), reaching their maxima then decreased until 6.4 kyr cal BP with several cooling events around 9.3, 8.6 and 8 kyr cal BP ([Fig. 4B](#)). A slight increase of temperatures occurred until 2.7 kyr cal BP. During the late Holocene, temperatures fluctuated around the modern value (7.2 °C). The mean temperature of the warmest month (MTWA) showed similar trends with a rapid increase of temperatures at the onset of the Holocene ([Fig. 4C](#)) and a thermal optimum to 6.9 kyr cal BP (mean=18.6 °C) before temperatures decreased until 6.4 kyr cal BP. Temperatures increased between 6.4 and 2.8 kyr cal BP and fluctuated around 16.1 °C during

the late Holocene. The growing degree days above 5 °C (GDD5), a measure of the cumulative temperature ([Prentice et al., 1992](#)), followed a very similar pattern with a maximum reached at 10 kyr cal BP then a decrease to 6.4 kyr cal BP ([Fig. 4D](#)). The mean temperature of the coldest month (MTCO) indicated a rise at the beginning of the Holocene (+1.3 °C between 10.6 and 10 kyr cal BP), followed by a decrease until around 8 kyr cal BP. Then, they rose again and remained around 0 °C prior to decreasing again from 2.9 to 1.3 kyr cal BP and finally rising (+2.2 °C until modern time) ([Fig. 4E](#)).

##### 3.2.2. Weighted-averaging partial least squares method

The mean annual temperature for the entire Holocene was 11.3 °C, i.e. 4.1 °C above the modern value. The maximum of 14 °C and a minimum of 7.6 °C were reached, respectively, at 7.8 and 1.7 kyr cal BP. The annual temperatures increased abruptly from 10.6 to 9.8 kyr cal BP then remained high until 7.4 kyr cal BP. The period between 7.4 and 6 kyr cal BP is marked by a cooling event, but the annual temperatures rose again at 6 kyr cal BP prior to decreasing regularly until 2 kyr cal BP and then oscillating around a mean value of 9.2 °C ([Fig. 4B](#)). The MTWA also showed a rapid increase from 10.6 to 10 kyr cal BP (+2.7 °C) then temperatures continued increasing until 7.4 kyr cal BP prior to a decrease until around 3.5 kyr cal BP and stabilizing around 17.7 °C with numerous rapid oscillations ([Fig. 4C](#)). The GDD5 followed a quasi-identical trend ([Fig. 4D](#)). The mean temperature of the coldest month (MTCO) varied in a similar way to the annual temperatures with values ranging from 8 to −1.6 °C ([Fig. 4E](#)).

### 4. Discussion

#### 4.1. *brGDGT* temperature record

##### 4.1.1. Evidence of a bias by source changes

The  $\Sigma\text{IIIa}/\Sigma\text{IIa}$  values indicate a gradual change of brGDGT sources through the Holocene from lacustrine to terrigenous origins ([Fig. 2A](#); [Martin et al., 2019](#)). Several short-term events of enhanced erosion occurred from 6 to 5.5, 2.8 to 2.5 and 2 to 0.2 kyr cal BP. They resulted from changes in vegetation cover from climatic and/or anthropogenic origin in particular from 2.8 kyr cal BP when human occupation of Lake St Front catchment became permanent with associated deforestation and agropastoralism ([Martin et al., 2019](#)). These events coincided with the occurrence of maxima in MBT, MBT', MBT'<sub>5Me</sub> and CBT values ([Fig. 2A–D](#)). This indicates a bias in brGDGT distributions linked with the increase of terrigenous brGDGTs. The soils of the Lake St Front catchment present a different pattern of brGDGT distributions from the lake sediments ([Martin et al., 2019](#)). As more terrigenous brGDGTs entered the lake, the brGDGT distribution of sediments changed and biased the indices and the reconstructed temperatures. To test the impact of changing brGDGT sources on temperature reconstruction, we applied several lacustrine and soil calibrations on modern catchment samples ( $n=18$ ) and core-tops sediment ( $n=7$ ) ([Fig. 5](#), [Table 1](#)).

The soil calibration of [Peterse et al. \(2012\)](#) applied to catchment samples provides the closest temperature compared to the measured one (modern MAAT=7.2 °C, [Fig. 5](#), [Table 1](#)). The lacustrine calibrations of [Sun et al. \(2011\)](#), [Loomis et al. \(2012\)](#) and [Russell et al. \(2018\)](#) provided core-top temperatures consistent with the monitored values ([Fig. 5](#), [Table 1](#)). Except for the calibration of [Russell et al. \(2018\)](#), all of the calibration equations based on the indices established with the new separation method of the 5-, 6- and 7-Me forms of brGDGTs ([De Jonge et al., 2013, 2014](#); [Ding et al., 2016](#)) provided temperatures inconsistent with the modern mean annual temperature observed in St Front ([Fig. 5](#)). Most of these are soil calibrations ([De Jonge et al., 2014](#); [Naafs et al., 2017](#)) as few



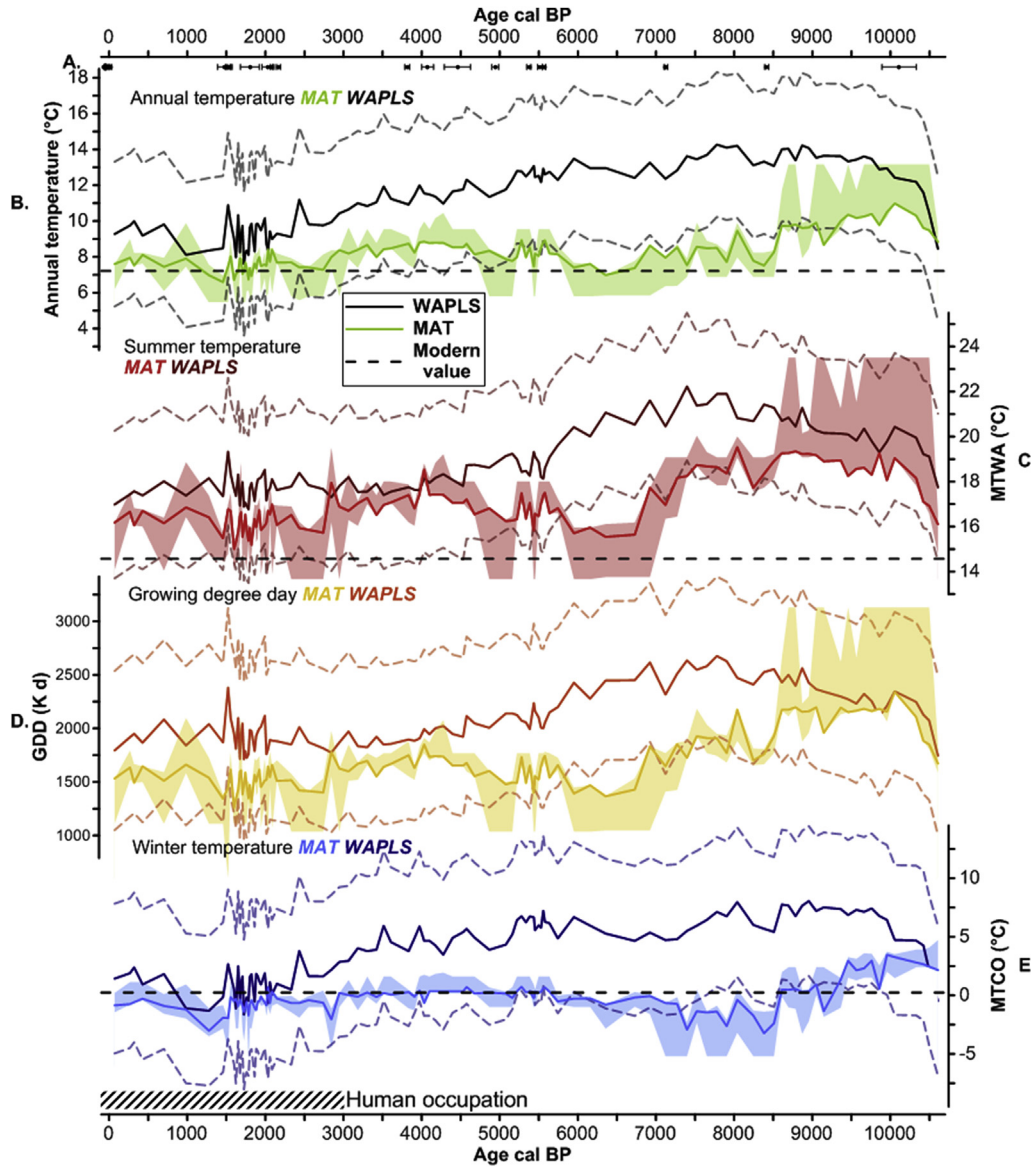


**Fig. 4. Paleoclimatic reconstructions from pollen.** Paleoclimatic parameters obtained with the Modern Analog Technique (MAT, light curves and shading for uncertainty) and Weighted Averaging Partial Least Squares (WAPLS, dark curves with uncertainty represented by the dashed lines) methods compared with the present mean annual, summer and winter temperatures at St Front (black dashed line). **A.**  $^{14}\text{C}$  calibrated ages and  $^{210}\text{Pb}$  dates (Martin et al., 2019). **B.** Annual temperature. **C.** Mean temperature of the warmest month (MTWA). **D.** Growing degree days (GDD). **E.** Temperature of the coldest month (MTCO). The period of permanent human occupation is marked by a hatched rectangle.

lacustrine calibrations have been developed (Table 2).

The calibrations of Loomis et al. (2012) and Russell et al. (2018) were developed for African lakes (Table 2). Although the calibration of Russell et al. (2018) uses the new separation method, the application of a calibration developed in settings without thermal seasonality to a European lake is questionable as the environmental conditions and hydrology of lakes are different. Furthermore, Dang et al. (2018) noted that brGDGT-producing communities can respond differently to environmental conditions and recommended the use of regional calibration as did Müller et al. (2018). Several studies also underlined that seasonality biases on brGDGT signal vary regionally (see Section 4.3.3). As there is no regional calibration for Europe, using the calibration of Sun et al. (2011) with the global coverage of its calibration data set could cancel these regional effects.

When soil calibrations are applied to the surface sediments, the modern temperature can be underestimated by as much as 4.1 °C

(Fig. 5, Table 1) as reported by many studies (e.g., Tierney and Russell, 2009; Blaga et al., 2010; Tierney et al., 2010; Zink et al., 2010; Loomis et al., 2011; Sun et al., 2011; Kaiser et al., 2015). Conversely, when lacustrine calibrations are applied to catchment samples, the modern temperature can be overestimated by as much as 4.8 °C (Fig. 5, Table 1). These mismatches result from the distribution differences between lake sediments and catchment samples due to in situ production. In particular, there is a greater abundance of hexamethylated brGDGTs (III) in sediments (Martin et al., 2019). The distribution difference of 5- and 6-Me isomers observed between soils and sediments (Martin et al., 2019) suggests that these isomers could also play a role in this distinct response to climatic parameters in the two environments (Dang et al., 2018). We conclude that the mixed terrigenous and lacustrine origins of brGDGTs present in sediments preclude the direct application of lake- or soil-based calibration.

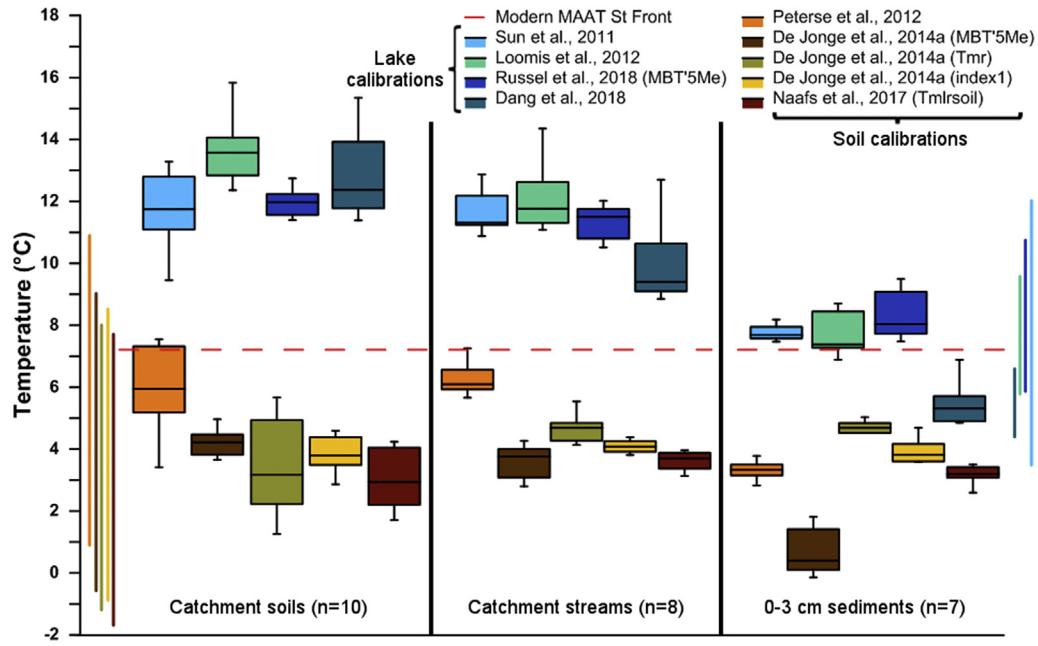


**Fig. 5. Test of several lake and soil calibrations on top sediments and catchment soils and streams of Lake St Front.** In this boxplot, each box presents the results of a calibration applied successively on three sample types appearing on the abscissa, catchment soils ( $n=10$ ) and streams ( $n=8$ ), and top sediments ( $n=7$ ) from short interface top cores from Lake St Front (see Fig. 1 for locations). Lake calibrations are in shades of blue. The red dashed line represents the instrumentally measured mean annual air temperature of Lake St Front. The vertical colored bars represent the root mean square errors associated with each calibration. (For interpretation of the references to color in this figure legend, the reader is referred to the Web version of this article.)

**Table 2**

Characteristics of the calibrations tested on Lake St Front samples (see Fig. 5). The notation [X] corresponds to the fractional abundance of X. RMSE = root mean square error.

Reference	Area	Sample type	Equations	$n$	$R^2$	RMSE (°C)
Sun et al. (2011)	Global	Lake sediments	$MAAT = 3.949 - 5.593 \times CBT + 38.213 \times MBT$	100	0.73	4.27
Loomis et al. (2012)	East Africa	Lake sediments	$MAAT = 22.77 - 33.58 \times [IIIa] - 12.88 \times [IIa]$ $- 418.53 \times [IIc] + 86.43 \times [Ib]$	111	0.94	1.9
Russell et al. (2018)	East Africa	Lake sediments	$MAAT = -1.21 + 32.42 \times MBT'_{5Me}$	65	0.92	2.44
Dang et al. (2018)	China	Lake sediments	$T_{growth} = -29.73 \times [IIIa]_{5Me} + 91.97 \times [IIIb]_{5Me}$ $- 551.02 \times [IIIc]_{5Me} + 22.65 \times [IIb]_{5Me}$ $+ 3.19 \times [Ib]_{5Me} - 4.23 \times [IIIa']_{6Me}$ $- 147.28 \times [IIIb']_{6Me} + 460.10 \times [IIIc']_{6Me}$ $- 14.59 \times [IIa']_{6Me} + 40.02 \times [IIb']_{6Me}$ $- 230.78 \times [IIc']_{6Me} + 7.54 \times [Ia]_{6Me}$ $+ 29.48 \times [Ic]_{6Me} + 12.73$	39	0.91	1.1
Peterse et al. (2012)	Global	Soils	$MAAT = 0.81 - 5.67 \times CBT + 31 \times MBT'$	176	0.59	5.0
De Jonge et al. (2014)	Global	Soils	$MAAT = -8.57 + 31.45 \times MBT'_{5Me}$	222	0.66	4.8
			$T_{mr}: MAAT = 7.17 + 17.1 \times [Ia] + 25.9 \times [Ib]$ $+ 34.4 \times [Ic] - 28.6 \times [IIa]$	222	0.68	4.6
			$MAAT = 5.05 + 14.86 \times \text{Index 1}$	222	0.67	4.7
Naafs et al. (2017)	Global	Soils	$MAAT_{mlrsoil} = 19.8 \times [Ia] + 31.1 \times [Ib]$ $- 23.4 \times [IIa] + 4.32$	350	0.62	4.7

#### 4.1.2. Correction with a binary mixing model

To account for changing sources of brGDGTs, we applied a binary mixing model based on the  $\Sigma IIIa/\Sigma IIa$  ratio following the approach of Sanchi et al. (2014), Ménot and Bard (2012) and Weijers et al. (2006b). Two end-members were defined, one for the soil catchment based on a mean of all the soil catchment samples of St Front ( $n=10$ ,  $\Sigma IIIa/\Sigma IIa = 0.33 \pm 0.09$ , Fig. 6A). The other was based on Holocene sediment samples for which  $\Sigma IIIa/\Sigma IIa$  exceeded the threshold value for aquatic production as defined by Xiao et al. (2016) ( $n=22$ ,  $\Sigma IIIa/\Sigma IIa = 1.04 \pm 0.07$ , Fig. 6A). The two end-members were mixed, adding a proportion of terrigenous brGDGTs to the lacustrine ones as follows:

$$[brGDGT - X]_{mix} = \alpha \times [brGDGT - X]_{lake} + (1 - \alpha) \times [brGDGT - X]_{soil} \quad (9)$$

with  $\alpha$ , the proportion of brGDGTs produced in the lake, varying from 0 to 1 and  $[brGDGT - X]$  successively corresponding to the fraction of each brGDGT. For each value of  $\alpha$ , the  $\Sigma IIIa/\Sigma IIa$  ratio was calculated (Fig. 6B). The modeled temperature bias was obtained by comparing the MAAT calculated from the mix composition using the calibration of Sun et al. (2011) with the temperature of the lacustrine end-member (Fig. 6B). For each sediment sample, the proportion of terrigenous brGDGTs then the temperature bias can be determined from the measured  $\Sigma IIIa/\Sigma IIa$  ratio using the mixing

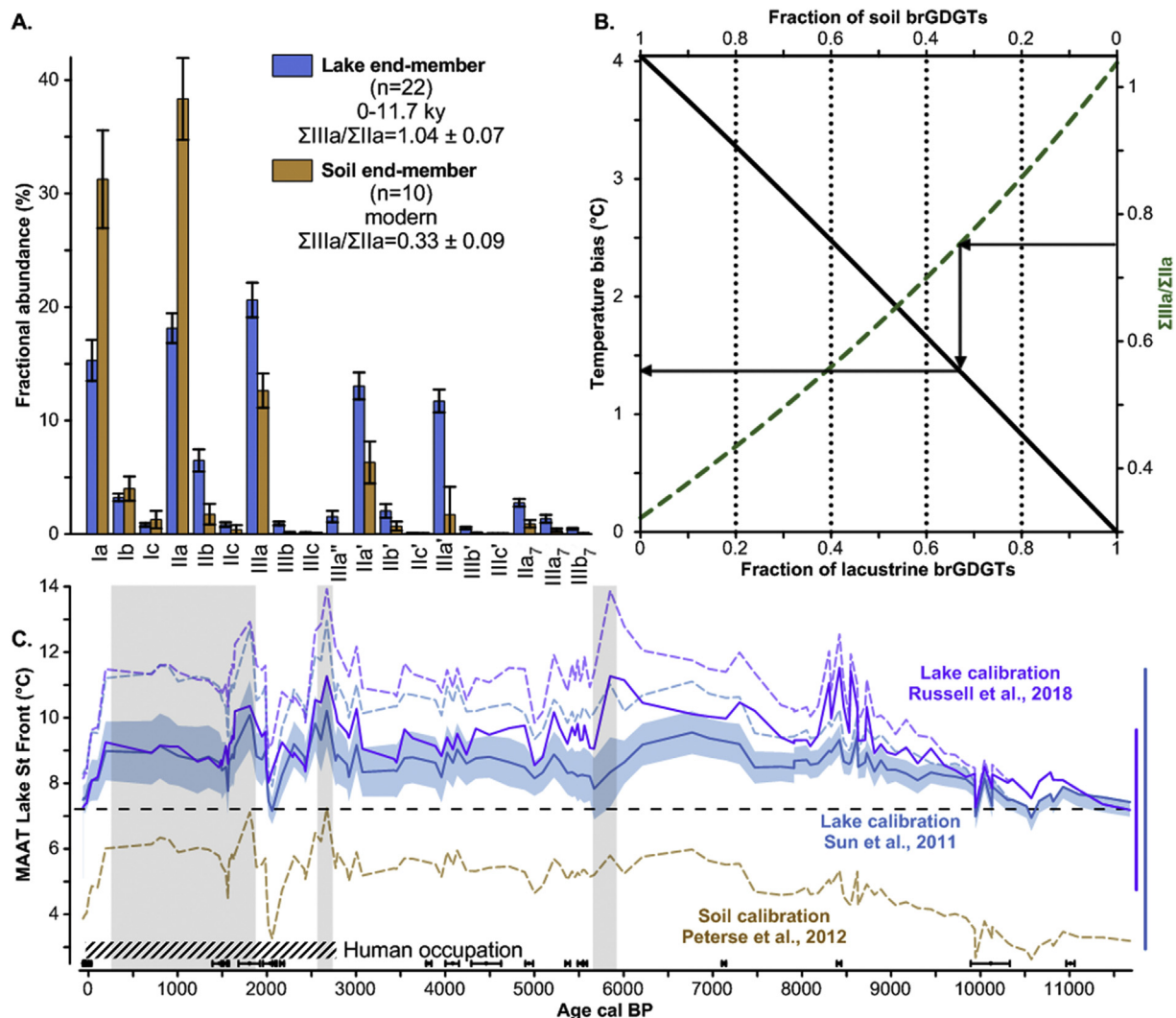


**Fig. 6. Binary mixing model and correction of terrigenous influence on MBT/CBT derived temperatures.** **A.** brGDGT distribution of lake sediment and soil end-members. **B.** Evolution of the temperature bias depending on the percentage of lacustrine brGDGTs (continuous line) and associated  $\Sigma IIIa/\Sigma Ia$  values (dashed line) in the case of the Sun et al. (2011) calibration. Arrows indicate an example of determination of the temperature bias from a measured  $\Sigma IIIa/\Sigma Ia$  value with this mixing model. **C.** Corrected mean annual air temperature (MAAT) obtained from the binary mixing model for Lake St Front with the Sun et al. (2011) and Russell et al. (2018) calibrations (blue and purple continuous line, respectively) with the error associated to the propagation of end-member variability for the Sun et al. (2011) calibration (blue shading) compared with the present mean annual temperature at St Front (black dashed line) and surrounded by annual temperatures reconstructed with the Sun et al. (2011, blue dashed curve), Russell et al. (2018, purple dashed line) and Peterse et al. (2012, brown dashed curve) calibrations. The vertical bars represent the error associated with the Sun et al. (2011) and Russell et al. (2018) calibrations (blue and purple lines, respectively). At the bottom,  $^{14}C$  calibrated ages and  $^{210}Pb$  dates appear as black circles (Martin et al., 2019). Shaded rectangles highlight the periods when  $\Sigma IIIa/\Sigma Ia$  values are below soil origin higher limit. The period of permanent human occupation is marked by a hatched rectangle. (For interpretation of the references to color in this figure legend, the reader is referred to the Web version of this article.)

model (Fig. 6B). The temperature obtained using the calibration of Sun et al. (2011) for each sample was corrected by subtracting the modeled bias (Sup Table 5). The corrected temperature values were bracketed by values obtained using the Sun et al. (2011) and Peterse et al. (2012) calibrations (Fig. 6C). They were used to constrain the maximal range of variations of the mixing model. The same method was used with the Russell et al. (2018) calibration. The temperatures from the surface sediment obtained with the Sun et al. (2011) and Russell et al. (2018) calibrations (7.5 and 7.3 °C, respectively) were very close to the modern value in Lake St Front (7.2 °C) validating the correction applied. The threshold of  $\Sigma IIIa/\Sigma Ia$ , defined from a database of marine sediments by Xiao et al. (2016) was used to delimit the aquatic brGDGT production realm and seems appropriate for lacustrine environments. In temperate lakes with in situ production, the temperature effect on the  $\Sigma IIIa/\Sigma Ia$  ratio seems too weak to preclude the use of this ratio to track past changes in

brGDGT sources (Martin et al., 2019).

The binary mixing model allowed correction of the input of terrigenous brGDGTs and the associated temperature bias which can reach 4 °C (Fig. 6B). With the corrections, the mean reconstructed Holocene brGDGT-inferred temperature was 8.5 and 9.1 °C for the Sun et al. (2011) and Russell et al. (2018) calibrations, respectively. For the Sun et al. (2011) calibration, the maximum of 10.2 °C is reached at 2.7 kyr cal BP and the minimum of 7 °C at 10.6 kyr cal BP (Fig. 6C). For the Russell et al. (2018) calibration, the maximum of 11.5 °C is reached at 8.4 kyr cal BP and the minimum of 7.2 at 11.7 kyr cal BP. The amplitude of the reconstructed temperatures through the Holocene was 3.3 and 4.3 °C for the Sun et al. (2011) and Russell et al. (2018) calibrations, respectively, consistent with the values inferred for the northern hemisphere from isotopes, biomarkers, pollen data and chironomid assemblages (Fig. 7B–H). The two lacustrine calibrations led to very similar

trends of the temperature evolution. However, the Russell et al. (2018) calibration led to higher temperatures during the early and mid-Holocene compared with results of the Sun et al. (2011) calibration. For the rest of the discussion, we only considered the results of the Sun et al. (2011) calibration as they are more consistent with the pollen reconstruction for St Front and other regional records (Fig. 7).

#### 4.2. Pollen temperature reconstructions

In contrast to the WAPLS, the MAT method is particularly well adapted to large data sets and has been extensively used for single site reconstructions (e.g., Peyron et al., 2005, 2017) and large-scale reconstructions of the Holocene climate (e.g., Bartlein et al., 2011; Mauri et al., 2015). The MAT method does not rely on a response function dominated by a single climate variable and thus allows reconstructions in areas where the composition of plant communities is limited by different parameters. However, the results show that the analogs selection for the early Holocene, though acceptable, could be improved as suggested by the high distances in the calculation of the MAT (Fig. S1). A possible explanation is that at the onset of the Holocene, the pollen diagram was dominated by *Corylus* (Fig. 3B, Sup Table 4) with percentages >55%. Surface samples dominated by very high percentages of *Corylus* are lacking in the modern pollen database in which some samples, with 25–35% of *Corylus* pollen from Italy, Ireland and Albania are available. This can bias the signal towards high temperature values. The analogs selection could be improved by the addition of pollen spectra dominated by thermophilous taxa such as *Corylus*, *Quercus* and *Fraxinus*.

The WAPLS is not an assemblage approach but it shows inconsistencies for the same time period. The temperature values obtained with the WAPLS appear clearly to be overestimated (Fig. 4A) and the method seems unsuitable for our large-scale database containing more than 3000 pollen samples from ecosystems ranging from Mediterranean vegetation to tundra. A locally focused calibration may improve the performance of the model and the reliability of the reconstruction (Montade et al., 2019). To sum up, we suggest that the reconstruction of the climate signal for the period 10,000–8500 cal BP inferred from the MAT and the WAPLS can be improved. The reconstruction for the Mid to Late Holocene appears to be more reliable (Fig. S1).

#### 4.3. Two independent records of an HTM in Lake St Front

Considering the uncertainties of the reconstructions, the overall trends of pollen- and brGDGT-inferred temperatures were similar through the Holocene. The temperatures reconstructed from brGDGTs and pollen using the MAT method are very similar (Fig. 7I and J). Their Holocene mean and maximal amplitude values are very close (8.3 °C/4.4 °C for the MAT method vs 8.5 °C/3.3 °C for brGDGTs) while the WAPLS method led to higher values (11.3 °C/6.7 °C). Comparing the temperatures reconstructed from brGDGTs and pollen with the MAT method through the Holocene, the difference did not exceed 3.5 °C in absolute value and is very close to zero from 6 to 3 kyr cal BP (Fig. 7K). The periods of discrepancy between both methods, 11–8.6, 7–6 and 2.8 kyr cal BP until present (Fig. 7K), will be discussed in the following sections. The values of annual temperatures obtained in St Front are also similar with the ones obtained from a Switzerland speleothem (Fig. 7H; Affolter et al., 2019).

When abrupt cold events are excluded, brGDGTs and pollen reconstructions both show a period of warmer temperatures than the mean Holocene values at the beginning of the interglacial even if the timing is not exactly similar (see Sections 4.3.1 and 4.3.2): between 8.7 and 6.2 kyr cal BP (Fig. 7J; maximal anomaly,  $\Delta T$ ,

of +1.1 °C for brGDGTs) and between 10 and 7–6 kyr (Fig. 7I; maximal  $\Delta T$  of +2.7 and +2.9 °C for MAT and WAPLS, respectively). The pattern of an early Holocene temperature maximum and subsequent decreasing temperatures is consistent with various regional temperature records based on independent proxies. Temperature reconstitutions from Austrian (Ilyashuk et al., 2011), Northern Italian (Samartin et al., 2017), Switzerland, German and French alpine lakes (Fig. 7G; Heiri et al., 2015) based on chironomid assemblages also present this pattern. The temperature evolution in St Front record is also consistent with German (Kluge et al., 2013) and Switzerland (Fig. 7H; Affolter et al., 2019) temperature reconstructions based on isotopic analysis of speleothems and the Mediterranean sea surface temperatures (SST) based on alkenones from the Alboran sea (Fig. 7F; Cacho et al., 1999; Leduc et al., 2010; Martrat et al., 2014). Northern European records also show a similar pattern even if the HTM is generally delayed from 2 to 3 kyr compared to mid-latitude records (e.g., Brown et al., 2012; Borzenkova et al., 2015). At the scale of the northern hemisphere, the temperature evolution at St Front is also consistent with Iceland mean annual temperature obtained from brGDGTs (Moossen et al., 2015), the Greenland temperature record based on combined nitrogen and argon isotope analyses (Fig. 7E; Kobashi et al., 2017), the North Atlantic SST based on Mg/Ca ratios (Rosenthal et al., 2017), the southwestern Chinese temperature obtained from brGDGTs (Ning et al., 2019) and the northern hemisphere temperatures synthesis from Marcott et al. (2013) (Fig. 7B). A cooling trend for the last 7 kyr is also recorded by brGDGTs in a Chinese loess-paleosol sequence (Zhao et al., 2018). At a more global scale, the occurrence of the HTM and the subsequent cooling trend is recorded in the Pacific Ocean (Rosenthal et al., 2013, 2017) and appears in the mean global ocean temperature reconstruction (Bereiter et al., 2018).

##### 4.3.1. Uncertainties on the HTM onset

The temperature rise at the HTM onset occurred earlier in the pollen-based curves than in the brGDGT-inferred signal (Fig. 7I–J). The initiation of the HTM around 10 kyr cal BP reconstructed from the St Front pollen data is consistent with most of the regional and global temperature records (Fig. 7; NGRIP Members et al., 2004; Ilyashuk et al., 2011; Marcott et al., 2013; Heiri et al., 2015; Kobashi et al., 2017; Samartin et al., 2017; Affolter et al., 2019). It also corresponds to the orbital-induced summer insolation maximum in the northern hemisphere (Fig. 7A).

In contrast, the Holocene climatic optimum was clearly delayed in the brGDGT-inferred MAAT. The increasing trend in GDGT-based temperatures was interrupted by a cold episode between 11.4 and 10 kyr cal BP and the warm phase only began at 8.7 kyr cal BP (Fig. 7J). This delay has also been observed in North America. The HTM began between 7 and 6 kyr cal BP in Northeast Canada while it was synchronous with the summer insolation maximum (between 11 and 9 kyr cal BP) in Alaska and northwest Canada (Kaufman et al., 2004). The late deglaciation of the Laurentide Ice Sheet (Carlson et al., 2008) may be responsible for this delay in North America and its influence on the timing of the HTM in Europe has been suggested (Renssen et al., 2009). Western Europe is particularly affected by this effect with a delay which can span up to 2000 years. The Fennoscandian Ice Sheet that persisted until 9 kyr cal BP (Lindén et al., 2006) also lead to a delayed HTM in Northern Europe (e.g., Brown et al., 2012; Borzenkova et al., 2015).

This delay was not recorded by pollen assemblages even though they have longer response times than brGDGTs (Weijers et al., 2010; Lauterbach et al., 2011). Pollen assemblages integrated the vegetation signal from the plateau and from the surrounding valleys characterized by higher temperatures. This could explain the higher temperatures obtained from pollen compared to brGDGTs



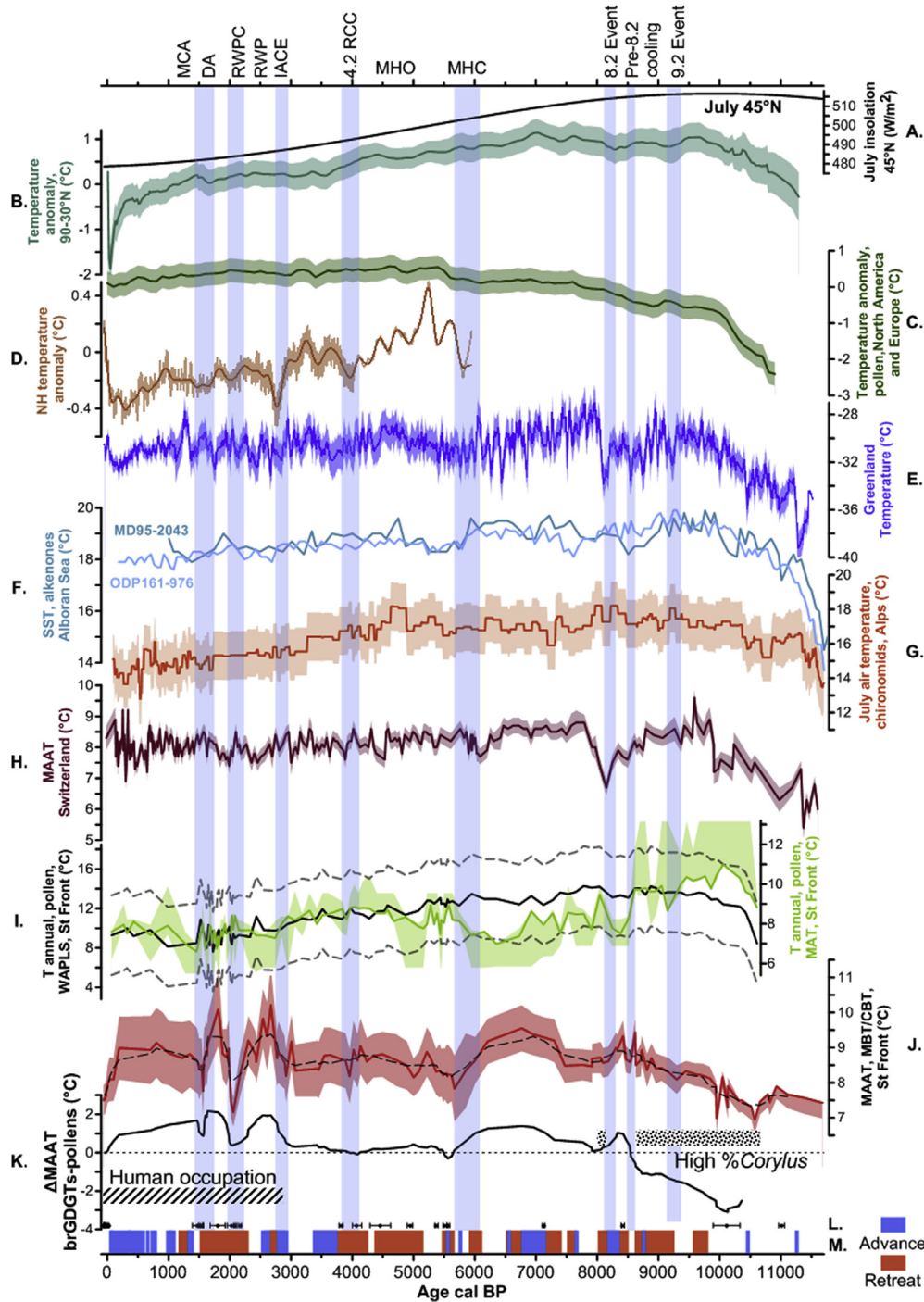


**Fig. 7. Holocene climatic variations in the northern hemisphere and a focus on Western Europe.** **A.** July insolation at 45°N (Laskar et al., 2004). **B.** Stacked temperature anomaly (from the AD 1961–1990 mean) for middle and high latitudes of the northern hemisphere obtained from a compilation of proxy-based temperature reconstructions with 1 $\sigma$  uncertainty (shading) from Marcott et al. (2013). **C.** Mean annual temperature reconstruction for North America and Europe based on fossil pollen data with 2.5 and 97.5% uncertainty bands (shading) from Marsicek et al. (2018). **D.** Temperature anomaly for the northern hemisphere obtained from a compilation of proxy-based temperature reconstructions from land areas and its 200-year Butterworth low-pass filtered values (brown line) from Pei et al. (2017). **E.** Reconstructed temperature from argon and nitrogen isotopes for Greenland with 2 $\sigma$  error bands from Kobashi et al. (2017). **F.** Sea surface temperature provided by relative proportion of the di- and tri-alkenones of 37 carbons from ODP Site 161-976 and sediment core MD95-2043 (Cacho et al., 1999; Martrat et al., 2014). **G.** Spliced and stacked chironomid-based reconstruction for the northern and central Alpine area at 1000 m from Heiri et al. (2015) with standard error estimates (shading). **H.** Mean annual air temperature obtained from fluid inclusions in speleothems from Milandre Cave in Switzerland (Affolter et al., 2019) with uncertainty (shading). **I.** Mean annual temperature reconstructed from pollen of Lake St Front with Weighted Averaging Partial Least Squares (WAPLS, black curve) and Modern Analog Technique (MAT, green curve) methods with its uncertainty (grey dashed lines and green shading, respectively). **J.** Corrected mean annual air temperature (MAAT) obtained from the binary mixing model with the Sun et al. (2011) calibration for Lake St Front (red continuous line) with the error associated to the propagation of end-member variability (red shading) and its running average on 5 points (black dashed line) compared with the mean Holocene temperature (black dotted line). **K.** Difference between the mean annual temperatures obtained from brGDGTs and pollen with the MAT method, the black dashed line indicates equality between both results. **L.**  $^{14}\text{C}$  calibrated ages and  $^{210}\text{Pb}$  dates for Lake St Front for the Holocene (Martin et al., 2019). **M.** Advances (blue rectangles) and recessions (orange rectangles) of Alps glaciers (Holzhauser et al., 2005; Joerin et al., 2006; Nicolussi and Patzelt, 2000; Solomina et al., 2015). Blue shaded rectangles correspond to cold events. The period of permanent human occupation is marked by a hatched rectangle. The dotted rectangle shows the period with high *Corylus* percentages. MHC=Mid-Holocene Cooling, MHO=Mid-Holocene Optimum, RCC=Rapid

which provide a more local signal (Fig. 7I–J). The pollen-inferred climate reconstruction could also be biased towards higher temperatures at the onset of the Holocene (10–8.6 kyr cal BP) by the high percentages of *Corylus* (Fig. 3B). The relationships between plant abundances and pollen data are not linear because of biases such as differences between plant species in pollen production and dispersal ability (e.g., [Prentice and Parsons, 1983](#)). *Corylus* in particular, is a thermophilous taxon which produces large quantities of pollen in open areas ([Bégeot, 1998](#)) and can bias reconstructed temperatures towards higher values. Other biases of pollen signal can also play a role. These include atmospheric conditions, especially wind speed and direction (e.g., [Andersen, 1974](#)), or a bias towards summer temperatures as the temperature peak is synchronous with maximum summer insolation in the northern hemisphere (Fig. 7A and I).

A bias towards cooler temperatures in the brGDGT-inferred signal could also be involved. The lag of the HTM in the brGDGT signal could be due to a change in the brGDGT-producing communities. The exploratory study of [De Jonge et al. \(2019\)](#) suggests that temperature changes affect brGDGT signatures in soils only after a change in the communities. The delay induced by this change can reach more than a decade ([DeAngelis et al., 2015](#)). The modification of the communities could also only occur when temperature change reaches a threshold ([De Jonge et al., 2019](#)).

The difference of timing of the two signals could result from a combination of a cold bias of brGDGTs and a warm bias of pollen, and the beginning of the HTM likely occurred between the two individual starting points.

#### 4.3.2. A synchronous HTM termination?

Similar to the brGDGT-based MAAT, the MAAT reconstructed from pollen using WAPLS method and the pollen-inferred summer temperatures show trends consistent with summer temperature records from the Alps and with northern hemisphere temperatures synthesized by [Marcott et al. \(2013\)](#). There was relative temperature stability before a decrease (Fig. 7B, F–J). Annual temperatures inferred from pollen using the MAT method start to decrease earlier, as soon as the temperature maximum was reached at 10 kyr cal BP. This may be due to the *Corylus* dominance during the early Holocene which biased temperature towards higher values (Fig. 7I). However, an early cooling pattern after reaching maximal temperature values, (as soon as 8 kyr cal BP), also exists in Greenland (Fig. 7E).

The timing of the decrease which marks the end of the HTM varies among records, but it seems to have occurred between 7 and 5 kyr cal BP (Table 3, Fig. 7). In our records, the end of the HTM occurred earlier in the pollen reconstruction obtained with the MAT method (at 7 kyr cal BP) than in the brGDGTs and the WAPLS reconstructions (Fig. 7I–J). Similarly other regional paleoclimatic archives recorded a late end of the HTM, around 6 kyr cal BP (Fig. 7F and H; [Samartin et al., 2017](#)). The Alps glaciers also showed a period of advances from 6.5 to 5.5 kyr cal BP (Fig. 7M; [Nicolussi and Patzelt, 2000](#); [Solomina et al., 2015](#)). However, several temperature reconstructions recorded a short cooling at 7 kyr cal BP (Fig. 7E–H; [Samartin et al., 2017](#)) which is also visible in the temperature signal inferred from pollen with the WAPLS method (Fig. 7I). This cooling seems to have been amplified by the MAT method which has a different sensitivity compared to the WAPLS (see Section 4.1.2). More methods based on pollen data such as Inverse Modelling ([Guiot et al., 2000](#)) or Boosted regression trees ([Salonen et al., 2019](#)) can be tested to improve the accuracy of the

climate reconstruction for this time period.

#### 4.3.3. Seasonality of the HTM temperature signal

This array of evidences of the HTM occurrence is in contradiction with climate models outputs (e.g., [Liu et al., 2014](#); [Zhang et al., 2018](#)) and temperature reconstructions obtained from pollen in North America and Europe (Fig. 7C; [Marsicek et al., 2018](#)), isotopic analysis of speleothems in Eurasia ([Baker et al., 2017](#)) and brGDGT analysis in Kamchatka peninsula (Russia; [Meyer et al., 2017](#)). These studies display a different pattern with a continuous warming through the entire Holocene and consider the HTM as the sign of a seasonal bias towards summer temperatures.

The trend in brGDGT-reconstructed temperatures at St Front through the Holocene shows good agreement with independent regional summer temperature records (Fig. 7G and J; [Ilyashuk et al., 2011](#); [Heiri et al., 2015](#); [Samartin et al., 2017](#)) and shows a HTM similar to the reconstruction compiled by [Marcott et al. \(2013\)](#) (Fig. 7B).

**4.3.3.1. Seasonality of the brGDGT signal.** Several studies have shown that there is no seasonal bias in brGDGT distributions and concentrations in soils, even for cold environments ([Weijers et al., 2011](#); [Lei et al., 2016](#); [Naafs et al., 2017](#); [Cao et al., 2018](#)). However, more and more studies suggest that reconstructed temperatures suffer from a bias towards the warm or growing season in brGDGT production in mid to high latitudes lakes ([Sun et al., 2011](#); [Shanahan et al., 2013](#); [Peterse et al., 2014](#); [Dang et al., 2018](#)), in tropical lakes ([Sobrinho et al., 2016](#); [Chu et al., 2017](#)), in marine sediments ([Rueda et al., 2009](#); [Moossen et al., 2015](#)), in French peat ([Huguet et al., 2010, 2013](#)) and even in soils ([Wang et al., 2014](#); [Ding et al., 2015](#); [Deng et al., 2016](#); [Nieto-Moreno et al., 2016](#); [Thomas et al., 2017](#)). The understanding of seasonal variations in brGDGT production is complicated by the fact that the brGDGT-producing bacteria are not yet fully identified (e.g., [Weijers et al., 2009](#); [Peterse et al., 2010](#); [Sinninghe Damsté et al., 2011, 2014, 2018](#)). This bias could reflect a seasonal trend in brGDGT production with an enhancement during the seasonal optimum for the growth of the brGDGT-producing bacteria. For example, at high latitudes, brGDGT production could be higher during the warm season, as bacterial growth is greater at higher temperatures and declines when soils are frozen. This would lead to a seasonal bias towards summer temperatures ([Rueda et al., 2009](#); [Huguet et al., 2010, 2013](#); [Sun et al., 2011](#); [Shanahan et al., 2013](#); [Peterse et al., 2014](#); [Moossen et al., 2015](#)). In arid and sub-humid environments, brGDGT production might be controlled by water availability and precipitation amount. It would thus be higher during the rainy season leading to a bias of reconstructed temperatures towards this season (e.g., [Dirghangi et al., 2013](#); [De Jonge et al., 2014](#); [Menges et al., 2014](#); [Nieto-Moreno et al., 2016](#)).

In lakes, brGDGT production could be more variable than in soils ([Peterse et al., 2014](#)). This production rests on primary production that is mainly dependent on nutrient availability. Nutrients are controlled by limnological processes and terrigenous inputs which are often seasonal ([Sobrinho et al., 2016](#); [Chu et al., 2017](#)). For example, [Chu et al. \(2017\)](#) presented evidence for a wintertime optimum in brGDGT production in a tropical monomictic Chinese lake in which the mixing process, and higher nutrient availability, occurs in winter. [Loomis et al. \(2014\)](#) also identified peaks of brGDGT production and export to sediments during fall and spring linked to seasonal mixing events in a dimictic lake. Even without seasonal mixing events, [Miller et al. \(2018\)](#) found seasonal brGDGT

**Table 3**  
Timing of the ending of the Holocene Thermal Maximum in different records from the northern hemisphere.

Record	HTM ending (kyr cal BP)	Reference
Northern Hemisphere annual temperatures synthesis	7	Marcott et al. (2013)
Greenland annual temperatures	Cooling since 8	Kobashi et al. (2017)
Alpine annual temperatures	6.4	Affolter et al. (2019)
Alpine summer temperatures	4.5	Heiri et al. (2015)
Alpine summer temperatures	6–5	Samartin et al. (2017)
Alboran Sea surface temperatures	6	Martrat et al. (2014), Cacho et al. (1999)
BrGDGT-based MAAT	6.2	This study
Pollen-inferred MAAT (WAPLS)	First decrease at 7.4, second at 6	
Pollen-inferred MAAT (MAT)	Cooling since 10, abrupt intensification at 7	
Summer temperatures pollen-inferred (MAT)	7	
Summer temperatures pollen-inferred (WAPLS)	Cooling start at 7, abrupt cooling at 6	

production peaking in fall. They also showed that brGDGT production varies as a function of depth and could record temperatures at varying depths.

The ice and snow covering of Lake St Front and its catchment (Fig. 1C) could lead to a seasonal bias in brGDGT production. However, when applying calibration to reconstruct annual temperatures, top sediments provide values consistent with monitored ones after correction for terrigenous inputs (Fig. 6C). This suggests that there is no seasonal bias towards summer temperatures. Variations of brGDGT production with depth seem unlikely in Lake St Front as its depth is shallow. Furthermore, the brGDGT-inferred MAAT shows almost no correlation with summer insolation at 45°N ( $R^2=0.10$ ,  $n=127$ ,  $p=0.0003$ ).

The brGDGT-inferred temperature signal of Lake St Front does not appear to be biased towards summer temperatures during the Holocene.

**4.3.3.2. Seasonality of the pollen signal.** The HTM also appears in pollen-inferred temperatures with both MAT and WAPLS methods in summer temperatures but also in annual temperatures and even in winter temperatures (Fig. 4). This suggests that HTM is not exclusively a summer signal. Annual and winter temperatures can be biased by summer temperature which constitutes a dominant variable (Rehfeld et al., 2016). However, the vegetation shift in St Front clearly indicates the occurrence of a warm period during the early Holocene, the HTM, followed by a cooling period during the mid-Holocene. There was an increase of the thermophilous forest during the early Holocene and a decline from 7.4 kyr BP as a mesophilous forest developed (Fig. 3; Martin et al., 2019). This climatic trend was also recorded by vegetation via the forest cover in the Alps and over all of Europe (Zanon et al., 2018).

**4.3.3.3. Influence of seasonal biases on the HTM.** Other records, which, *a priori*, are not biased towards summer temperatures, show the occurrence of an HTM. Several physically based seasonally unbiased records of temperature which show the HTM have been provided: for Greenland from combined nitrogen and argon isotopes (Fig. 7E; Kobashi et al., 2017) and from an inversion method in the Greenland Ice Core Project borehole (Dahl-Jensen et al., 1998), and the mean global ocean temperature based on noble gas isotopes (Bereiter et al., 2018). The few records in Western Europe (excluding the Mediterranean zone) which, *a priori*, are not biased towards summer temperatures all show the HTM (e.g., Mayer and Schwark, 1999; McDermott et al., 1999; Niggemann et al., 2003; Vollweiler et al., 2006; Badino et al., 2018). The temperature record obtained from fluid inclusions in a Switzerland speleothem which is potentially biased towards the cold season also present the HTM (Affolter et al., 2019).

The temperature signal of Lake St Front does not appear to be biased towards summer temperatures during the Holocene and

demonstrates, with other regional and more global records, that the HTM is not only a summer signal but, at least in mid-latitude Western Europe, corresponds to a general warm period. The growing number of records which are not biased towards summer and show the HTM, as well as the diversity of proxies and archives which records the HTM (e.g., Sup Table 1) seem to suggest that seasonal biases are not the source of the so-called Holocene conundrum (Liu et al., 2014). As suggested by Affolter et al. (2019), the large spatial heterogeneity of climate change during the Holocene, particularly between high and mid latitudes, may hamper a valid mean reconstruction for the overall Europe and northern hemisphere. This geographic heterogeneity could lead to inevitable biases in the synthesis of proxy-data records in particular when a geographic zone is over-represented.

#### 4.4. Millennial to centennial climate events during the Holocene

In addition to the long-term pattern, numerous rapid events with centennial durations have been recorded in Greenland ice cores and in other records through the Holocene (e.g., Bond et al., 2001; Mayewski et al., 2004; Wanner et al., 2011). Some of the well-known rapid climate changes in the northern hemisphere seem to correspond with rapid events often associated with marked temperature variations in the brGDGT-based temperature record (Table 4). These events correspond relatively well with advance and retreat phases of glaciers in the Alps (Fig. 7M) with some exceptions that may be linked with precipitation variability (Solomina et al., 2015). Despite slight differences in timing which may have resulted from the regional variability of rapid climate changes (e.g., Desprat et al., 2003; Viau et al., 2006; Jansen et al., 2007; Wanner et al., 2008), the events observed in St Front present a timing, temperature pattern and amplitude similar to other regional and global records based mainly on oceanic (Marcott et al., 2013) or continental data (Fig. 7B–J; Vollweiler et al., 2006; Pei et al., 2017; Marsicek et al., 2018; Affolter et al., 2019).

The rapid events depicted by the brGDGTs were also seen in our pollen-inferred climate reconstructions despite some minor lags or differences in amplitude (Fig. 7I–J). The major difference occurred in the timing of the mid-Holocene cooling which marked the end of the HTM (see section 4.3.2). Moreover, the amplitude of the 8.2 ka event was higher in the pollen-inferred temperature record obtained with the MAT method than in the other temperature records (−1.7 °C for the MAT method versus −0.9 °C and −0.8 °C, respectively with the WAPLS method and brGDGTs). The 9.2 ka event appeared with the MAT method (−2.2 °C, Fig. 7I) while it was not marked with the others. The differences of timing and amplitude between the different proxies could be due to the difference of the sampling interval between the two records or to sensitivity differences of the two proxies which have different response times and geographical scales of the signal recorded (see Section 4.3.1).



**Table 4**

Rapid climate changes identified in the brGDGT-based temperature record with their temperature variation, age interval and corresponding known event in the literature with associated age interval and reference.

Event	$\Delta T$ in St Front <sup>a</sup> (compared with mean Holocene temperature)	Age range in St Front (yr cal BP)	Age range in literature (yr cal BP)	Reference
Pre-8.2 ka cooling	-0.6 <sup>b</sup>	8600–8500	8800–8500	Kobashi et al. (2017)
8.2 ka event	-0.7 <sup>b</sup>	8400–8000	~8300–8100	Johnsen et al. (1992); Alley et al. (1997); Grootes and Stuiver (1997); Alley and Ágústssdóttir (2005); Kobashi et al. (2007); Rasmussen et al. (2007); Hede et al. (2010); Mercuri et al. (2011); Quillmann et al. (2012); Shuman (2012); Matero et al. (2017)
mid-Holocene cooling	-0.7	6200–5300	6000–5000	Sirocko et al. (1993); Sandweiss et al. (2001); Berglund (2003); Magny (2004); Magny and Haas (2004); Mayewski et al. (2004); Arbogast et al. (2006); Brooks (2006, 2012); Magny et al. (2006); Staubwasser and Weiss (2006); Shuman (2012)
mid-Holocene optimum	+0.5	4900–4000	5200–4000	Kobashi et al. (2017); Pei et al. (2017)
4.2 ka event	-0.3	4300–3900	4300–4100	Weiss et al. (1993); de Menocal (2001); Stanley et al. (2003); Staubwasser M. et al. (2003); Booth et al. (2005); Weiss (2012); Guo et al. (2018); Bini et al. (2019)
Iron Age Cold Epoch	-0.4	3000–2800	2900–2400 highly variable regionally	Panizza (1985); Landscheidt (1987); van Geel et al. (1997, 2000); Gutiérrez-Elorza and Peña-Monné (1998); Bond et al. (2001); Desprat et al. (2003); Gutiérrez et al. (2006); Swindles et al. (2007); Wanner et al. (2008); Martin-Puertas et al. (2012); Wang et al. (2012b); Kobashi et al. (2017)
Roman warm period	+1.7	2700–1600	2500–1600 highly variable regionally	Holzhauser et al. (2005); Vollweiler et al. (2006); Wang et al. (2012b); Moossen et al. (2015); Damnati et al. (2016)
Roman warm period cooling	-1.3	2200–2000	Minimum at ~2140	Wang et al. (2012b)
Dark Ages	-0.7	1600–1200	1500–1100 highly variable regionally	Hodell et al. (2001); Sicre et al. (2008); Büntgen et al. (2011, 2016); Moossen et al. (2015); Harper (2017)
Medieval Climate Anomaly	+0.6	~1100–700	~1000–700 highly variable regionally	Crowley and Lowery (2000); Desprat et al. (2003); Trouet et al. (2009); Graham et al. (2011); Geirsdóttir et al. (2013); Moossen et al. (2015); Lüning et al. (2017); Pei et al. (2017)

<sup>a</sup> The  $\Delta T$  were calculated from the Sun et al. (2011) calibration results after correction of the terrigenous effect.

<sup>b</sup>  $\Delta T$  calculated in comparison with the mean temperature of the HTM.

From 2.8 kyr cal BP until now, the increase of human activities around the lake imprinted the palynological record (Fig. 3A; Martin et al., 2019). The important decline of arboreal pollen denotes deforestation and the increased presence of anthropogenic taxa such as nitrophilous and cereal taxa indicate agropastoralism. The climate signal obtained from pollen for this period must therefore be carefully considered as it is potentially biased.

From 200 yr cal BP until the present time, the temperature record obtained from brGDGTs shows a cooling trend (Fig. 7J). This trend is not consistent with known records from the literature nor with instrumental data which show a warming trend since 1880 (Fig. 7B–H; Météo-France database <https://donneespubliques.meteofrance.fr>, PAGES 2k Consortium et al., 2013). Other studies based on brGDGTs have found low temperature values in surface lacustrine sediments and they do not show evidence for the recent warming (Sinninghe Damsté et al., 2012; Loomis et al., 2014; Miller et al., 2018). Miller et al. (2018) suggested that an ecological change due to anthropogenic activities could be responsible for this signal perturbation. Anthropogenic activities could be impacting the communities of brGDGT-producing bacteria and perturbing the temperature signal recorded.

## 5. Conclusions

The brGDGTs and pollen assemblages in the sediments of Lake St Front were studied to provide independent and robust quantitative estimates of annual temperatures during the Holocene. The study of modern samples demonstrates the overestimation of temperatures when using lacustrine calibrations on soil brGDGTs. The use of a binary mixing model allowed us to correct the temperature bias caused by the terrigenous inputs. This study highlights the importance of identifying the sources of brGDGTs in lake sediments

and their evolution through time as they can induce a bias of up to 4 °C. The lacustrine calibration of Sun et al. (2011) appeared to be the most appropriate to reconstruct past temperatures in St Front as the absolute values of the temperature obtained were more consistent with pollen-inferred temperatures and regional records than the African calibration of Russell et al. (2018) based on the new separation method. There is a need for local calibrations in Europe using the newly described indices based on the new chromatographic method.

The annual temperature signals reconstructed from both brGDGTs and pollen agree well with regional and global temperature reconstructions based on various proxies. They both show an early Holocene temperature maximum and a subsequent cooling until present. This is in agreement with independent proxies and regional and global records. The temperatures reconstructed from brGDGTs and the pollen-based MAT method are similar, while the WAPLS method show similar trends but produced higher temperatures. The timing of the beginning and the end of the HTM is also slightly different according to the method used for reconstruction and the biases that can be associated with it. Using a multi-proxy and multi-method approach allowed to identify the specific biases of each method and to compare with confidence our record to others on a regional scale. There is no evidence for a bias towards summer temperature either in the brGDGTs signal or in the pollen signal. At least in Western Europe, the HTM seems to correspond not only to a summer temperature signal but also to a general warm period. Seasonal biases unlikely explain the Holocene conundrum. Large spatial heterogeneities in temperature patterns could be a source of error when proxy-based records are aggregated to produce large-scale synthesis. At the millennial to centennial scales, both proxies have recorded the main known climatic events.



## Data availability

Data are provided in the supplementary material.

## Declaration of competing interest

The authors declare no competing interests.

## Acknowledgments

We thank an anonymous reviewer for his comments which improved the manuscript. We thank François Soubiran and Nicolas Lafon for their help with error propagation calculation and Emmanuel Guillerme for his help with the Mathematica software to produce the map in Fig. 1A. Qing Pei and Oliver Heiri are acknowledged for kindly supplying data. The work at CEREGE was supported by the Collège de France. Additional financial support was provided by the BNP Paribas Foundation (Climate Initiative – project CPATEMP). This is an ISEM contribution n° ISEM 2019-261.

## Appendix A. Supplementary data

Supplementary data to this article can be found online at <https://doi.org/10.1016/j.quascirev.2019.106109>.

## References

- Affolter, S., Häuselmann, A., Fleitmann, D., Edwards, R.L., Cheng, H., Leuenberger, M., 2019. Central Europe temperature constrained by speleothem fluid inclusion water isotopes over the past 14,000 years. *Sci. Adv.* 5, eaav3809 <https://doi.org/10.1126/sciadv.aav3809>.
- Alley, R.B., Mayewski, P.A., Sowers, T., Stuiver, M., Taylor, K.C., Clark, P.U., 1997. Holocene climatic instability: a prominent, widespread event 8200 yr ago. *Geology* 25, 483–486. [https://doi.org/10.1130/0091-7613\(1997\)025<0483:HCIAPW>2.3.CO;2](https://doi.org/10.1130/0091-7613(1997)025<0483:HCIAPW>2.3.CO;2).
- Alley, R.B., Ágústssdóttir, A.M., 2005. The 8k event: cause and consequences of a major Holocene abrupt climate change. *Quat. Sci. Rev.* 24, 1123–1149. <https://doi.org/10.1016/j.quascirev.2004.12.004>.
- Andersen, S.T., 1974. Wind conditions and pollen deposition in a mixed deciduous forest: I. Wind conditions and pollen dispersal. *Grana* 14, 57–63. <https://doi.org/10.1080/0017317409429894>.
- Andrieu, V., Bonifay, E., Reille, M., Roujati, A., Thouveny, N., 1995. Lac de St Front. In: *Quaternary Field Trips in Central Europe: The International Union for Quaternary Research, XIV International Congress*, pp. 1513–1518.
- Arbogast, R.-M., Jacomet, S., Magny, M., Schibler, J., 2006. The significance of climate fluctuations for lake level changes and shifts in subsistence economy during the late Neolithic (4300–2400 BC) in central Europe. *Veg. Hist. Archaeobotany* 15, 403–418. <https://doi.org/10.1007/s00334-006-0053-y>.
- Berglund, B.E., 2003. Human impact and climate changes—synchronous events and a causal link? *Quat. Int.* 105, 7–12. [https://doi.org/10.1016/S1040-6182\(02\)00144-1](https://doi.org/10.1016/S1040-6182(02)00144-1). Environmental variability in East and West Eurasia.
- Badino, F., Ravazzi, C., Vallè, F., Pini, R., Aceti, A., Brunetti, M., Champvillair, E., Maggi, V., Maspero, F., Perego, R., Orombelli, G., 2018. 8800 years of high-altitude vegetation and climate history at the Rutor Glacier forefield, Italian Alps. Evidence of middle Holocene timberline rise and glacier contraction. *Quat. Sci. Rev.* 185, 41–68. <https://doi.org/10.1016/j.quascirev.2018.01.022>.
- Baker, J.L., Lachniet, M.S., Chervyatsova, O., Asmerom, Y., Polyak, V.J., 2017. Holocene warming in western continental Eurasia driven by glacial retreat and greenhouse forcing. *Nat. Geosci.* 10, 430–435. <https://doi.org/10.1038/ngeo2953>.
- Bartlein, P.J., Harrison, S.P., Brewer, S., Connor, S., Davis, B.A.S., Gajewski, K., Guiot, J., Harrison-Prentice, T.J., Henderson, A., Peyron, O., 2011. Pollen-based continental climate reconstructions at 6 and 21 ka: a global synthesis. *Clim. Dyn.* 37, 775–802. <https://doi.org/10.1007/s00382-010-0904-1>.
- Bégeot, C., 1998. Le comportement pollinique du Noisetier (*Corylus avellana*), son rôle comme indicateur d'impacts anthropiques? L'exemple d'un transect dans le sud du Jura. *Acta Bot. Gall.* 145, 271–279. <https://doi.org/10.1080/12538078.1998.10516307>.
- Bendle, J.A., Weijers Johan, W.H., Maslin Mark, A., Sinninghe Damsté, J.S., Stefan, Schouten, Hopmans Ellen, C., Boot Christopher, S., Pancost Richard, D., 2010. Major changes in glacial and Holocene terrestrial temperatures and sources of organic carbon recorded in the Amazon fan by tetraether lipids. *Geochim. Geophys. Geosyst.* 11, Q12007. <https://doi.org/10.1029/2010GC003308>.
- Bereiter, B., Shackleton, S., Baggenstos, D., Kawamura, K., Severinghaus, J., 2018. Mean global air temperatures during the last glacial transition. *Nature* 553, 39–44. <https://doi.org/10.1038/nature25152>.
- Bini, M., Zanchetta, G., Persoiu, A., Cartier, R., Català, A., Cacho, I., Dean, J.R., Rita, F.D., Drysdale, R.N., Finnè, M., Isola, I., Jalali, B., Lirer, F., Magri, D., Masi, A., Marks, L., Mercuri, A.M., Peyron, O., Sadori, L., Sicre, M.-A., Welc, F., Zielhofer, C., Brisset, E., 2019. The 4.2 ka BP event in the Mediterranean region: an overview. *Clim. Past* 15, 555–577. <https://doi.org/10.5194/cp-15-555-2019>.
- Birks, H.J.B., Ter Braak, C.J.F., Line, J.M., Juggins, S., Stevenson, A.C., 1990. Diatoms and pH reconstruction. *Philos. Trans. R. Soc. Lond. B* 327, 263–278. <https://doi.org/10.1098/rstb.1990.0062>.
- Blaga, C.I., Reichert, G.-J., Schouten, S., Lotter, A.F., Werne, J.P., Kosten, S., Mazzeo, N., Lacerot, G., Sinninghe Damsté, J.S., 2010. Branched glycerol dialkyl glycerol tetraethers in lake sediments: can they be used as temperature and pH proxies? *Org. Geochem.* 41, 1225–1234. <https://doi.org/10.1016/j.orggeochem.2010.07.002>.
- Bond, G., Kromer, B., Beer, J., Muscheler, R., Evans, M.N., Showers, W., Hoffmann, S., Lotti-Bond, R., Hajdas, I., Bonani, G., 2001. Persistent solar influence on North Atlantic climate during the Holocene. *Science* 294, 2130–2136. <https://doi.org/10.1126/science.1065680>.
- Booth, R.K., Jackson, S.T., Forman, S.L., Kutzbach, J.E., Bettis III, E.A., Kreigs, J., Wright, D.K., 2005. A severe centennial-scale drought in midcontinental North America 4200 years ago and apparent global linkages. *Holocene* 15, 321–328. <https://doi.org/10.1191/0959683605hl825ft>.
- Borzenkova, I., Zorita, E., Borisova, O., Kalniņa, L., Kisielienė, D., Koff, T., Kuznetsov, D., Lemdahl, G., Sapelko, T., Stancikaitė, M., 2015. Climate change during the Holocene (past 12,000 years). In: *Second Assessment of Climate Change for the Baltic Sea Basin*. Springer, pp. 25–49. [https://doi.org/10.1007/978-3-319-16006-1\\_2](https://doi.org/10.1007/978-3-319-16006-1_2).
- Brooks, N., 2006. Cultural responses to aridity in the Middle Holocene and increased social complexity. *Quat. Int.* 151, 29–49. <https://doi.org/10.1016/j.quaint.2006.01.013>.
- Brooks, N., 2012. Beyond collapse: climate change and causality during the Middle Holocene Climatic Transition, 6400–5000 years before present. *Geogr. Tidsskr. Dan. J. Geogr.* 112, 93–104. <https://doi.org/10.1080/00167223.2012.741881>.
- Brown, K.J., Seppä, H., Schoups, G., Fausto, R.S., Rasmussen, P., Birks, H.J.B., 2012. A spatio-temporal reconstruction of Holocene temperature change in southern Scandinavia. *Holocene* 22, 165–177. <https://doi.org/10.1177/0959683611414926>.
- Buckles, L.K., Weijers, J.W., Verschuren, D., Sinninghe Damsté, J.S., 2014a. Sources of core and intact branched tetraether membrane lipids in the lacustrine environment: anatomy of Lake Challa and its catchment, equatorial East Africa. *Geochim. Cosmochim. Acta* 140, 106–126. <https://doi.org/10.1016/j.gca.2014.04.042>.
- Buckles, L.K., Weijers, J.W.H., Tran, X.-M., Waldron, S., Sinninghe Damsté, J.S., 2014b. Provenance of tetraether membrane lipids in a large temperate lake (Loch Lomond, UK): implications for glycerol dialkyl glycerol tetraether (GDGT)-based palaeothermometry. *Biogeosciences* 11, 5539–5563. <https://doi.org/10.5194/bg-11-5539-2014>.
- Büntgen, U., Tegel, W., Nicolussi, K., McCormick, M., Frank, D., Trouet, V., Kaplan, J.O., Herzog, F., Heussner, K.-U., Wanner, H., 2011. 2500 years of European climate variability and human susceptibility. *Science* 331, 578–582. <https://doi.org/10.1126/science.1197175>.
- Büntgen, U., Myglan, V.S., Ljungqvist, F.C., McCormick, M., Di Cosmo, N., Sigl, M., Jungclauss, J., Wagner, S., Krusic, P.J., Esper, J., 2016. Cooling and societal change during the late antique little ice age from 536 to around 660 AD. *Nat. Geosci.* 9, 231–236. <https://doi.org/10.1038/ngeo2652>.
- Cacho, I., Grimalt, J.O., Pelejero, C., Canals, M., Sierro, F.J., Flores, J.A., Shackleton, N., 1999. Dansgaard-Oeschger and Heinrich event imprints in Alboran sea paleo-temperatures. *Paleoceanography* 14, 698–705. <https://doi.org/10.1029/1999PA000044>.
- Cao, M., Rueda, G., Rivas-Ruiz, P., Trapote, M.C., Henriksen, M., Vegas-Villarrubia, T., Rosell-Melé, A., 2018. Branched GDGT variability in sediments and soils from catchments with marked temperature seasonality. *Org. Geochem.* 122, 98–114. <https://doi.org/10.1016/j.orggeochem.2018.05.007>.
- Carles, J., 1956. Notice détBulletin du Service de la Carte de la Phytogéographique. *Série A. Cartailée de la feuille 59 – Le Puy, de la carte de la végétation de la France au 1/200 000ème. e de la Végétation au 200 000ème.* CNRS, pp. 51–80.
- Carlson, A.E., LeGrande, A.N., Oppo, D.W., Came, R.E., Schmidt, G.A., Anslow, F.S., Licciardi, J.M., Obbink, E.A., 2008. Rapid early Holocene deglaciation of the Laurentide ice sheet. *Nat. Geosci.* 1, 620–624. <https://doi.org/10.1038/ngeo285>.
- Chu, G., Sun, Q., Zhu, Q., Shan, Y., Shang, W., Ling, Y., Su, Y., Xie, M., Wang, X., Liu, J., 2017. The role of the Asian winter monsoon in the rapid propagation of abrupt climate changes during the last deglaciation. *Quat. Sci. Rev.* 177, 120–129. <https://doi.org/10.1016/j.quascirev.2017.10.014>.
- Combouret-Nebout, N., Peyron, O., Bout-Roumazielles, V., Goring, S., Dormoy, I., Joannin, S., Sadori, L., Siani, G., Magny, M., 2013. Holocene vegetation and climate changes in the central Mediterranean inferred from a high-resolution marine pollen record (Adriatic Sea). *Clim. Past* 9, 2023–2042. <https://doi.org/10.5194/cp-9-2023-2013>.
- Crowley, T.J., Lowery, T.S., 2000. How warm was the medieval warm period? *AMBIO J. Hum. Environ.* 29, 51–54. <https://doi.org/10.1579/0044-7447-29.1.51>.
- Dahl-Jensen, D., Mosegaard, K., Gundestrup, N., Clow, G.D., Johnsen, S.J., Hansen, A.W., Balling, N., 1998. Past temperatures directly from the Greenland ice sheet. *Science* 282, 268–271. <https://doi.org/10.1126/science.282.5387.268>.
- Damnati, B., Etebaai, I., Benjilani, H., El Khoudri, K., Reddad, H., Taieb, M., 2016. Sedimentology and geochemistry of lacustrine terraces of three Middle Atlas lakes: Paleohydrological changes for the last 2300 cal BP in Morocco (western Mediterranean region). *Quat. Int.* 404, 163–173. <https://doi.org/10.1016/j.quaint.2016.01.013>.

- j.quaint.2015.10.038.
- Dang, X., Ding, W., Yang, H., Pancost, R.D., Naafs, B.D.A., Xue, J., Lin, X., Lu, J., Xie, S., 2018. Different temperature dependence of the bacterial brGDGT isomers in 35 Chinese lake sediments compared to that in soils. *Org. Geochem.* 119, 72–79. <https://doi.org/10.1016/j.orggeochem.2018.02.008>.
- Davis, B.A., Brewer, S., Stevenson, A.C., Guiot, J., 2003. The temperature of Europe during the Holocene reconstructed from pollen data. *Quat. Sci. Rev.* 22, 1701–1716. [https://doi.org/10.1016/S0277-3791\(03\)00173-2](https://doi.org/10.1016/S0277-3791(03)00173-2).
- Davtian, N., Bard, E., Ménot, G., Fagault, Y., 2018. The importance of mass accuracy in selected ion monitoring analysis of branched and isoprenoid tetraethers. *Org. Geochem.* 118, 58–62. <https://doi.org/10.1016/j.orggeochem.2018.01.007>.
- DeAngelis, K.M., Pold, G., Topçuoğlu, B.D., van Diepen, L.T.A., Varney, R.M., Blanchard, J.L., Melillo, J., Frey, S.D., 2015. Long-term forest soil warming alters microbial communities in temperate forest soils. *Front. Microbiol.* 6 <https://doi.org/10.3389/fmicb.2015.00104>.
- de Beaulieu, J.L., Pons, A., Reille, M., 1984. Recherches pollenanalytiques sur l'histoire de la végétation des monts du Velay, Massif central, France. *Diss. Bot.* 72, 45–70. [https://doi.org/10.1016/0034-6667\(85\)90028-4](https://doi.org/10.1016/0034-6667(85)90028-4).
- de Beaulieu, J.-L., Pons, A., Reille, M., 1988. Histoire de la végétation, du climat et de l'action de l'homme dans le Massif Central français depuis 15 000 ans. *Trav. Sect. Sci. Tech. Inst. Fr. Pondichery* 25, 27–32.
- de Beaulieu, J.-L., Reille, M., 1992. The last climatic cycle at La Grande Pile (Vosges, France) a new pollen profile. *Quat. Sci. Rev.* 11, 431–438. [https://doi.org/10.1016/0277-3791\(92\)90025-4](https://doi.org/10.1016/0277-3791(92)90025-4).
- De Jonge, C., Hopmans, E.C., Stadnitskaia, A., Rijpstra, W.I.C., Hofland, R., Tegelaar, E., Sinninghe Damsté, J.S., 2013. Identification of novel penta- and hexamethylated branched glycerol dialkyl glycerol tetraethers in peat using HPLC–MS<sup>2</sup>, GC–MS and GC–SMB–MS. *Org. Geochem.* 54, 78–82. <https://doi.org/10.1016/j.orggeochem.2012.10.004>.
- De Jonge, C., Hopmans, E.C., Zell, C.I., Kim, J.-H., Schouten, S., Sinninghe Damsté, J.S., 2014. Occurrence and abundance of 6-methyl branched glycerol dialkyl glycerol tetraethers in soils: implications for palaeoclimate reconstruction. *Geochim. Cosmochim. Acta* 141, 97–112. <https://doi.org/10.1016/j.gca.2014.06.013>.
- De Jonge, C., Radujković, D., Sigurdsson, B.D., Weedon, J.T., Janssens, I., Peterse, F., 2019. Lipid biomarker temperature proxy responds to abrupt shift in the bacterial community composition in geothermally heated soils. *Org. Geochem.* 137, 103897. <https://doi.org/10.1016/j.orggeochem.2019.07.006>.
- de Menocal, P.B., 2001. Cultural responses to climate change during the late Holocene. *Science* 292, 667–673. <https://doi.org/10.1126/science.1059287>.
- Deng, L., Jia, G., Jin, C., Li, S., 2016. Warm season bias of branched GDGT temperature estimates causes underestimation of altitudinal lapse rate. *Org. Geochem.* 96, 11–17. <https://doi.org/10.1016/j.orggeochem.2016.03.004>.
- Desprat, S., Goni, M.F.S., Loutre, M.-F., 2003. Revealing climatic variability of the last three millennia in northwestern Iberia using pollen influx data. *Earth Planet. Sci. Lett.* 213, 63–78. [https://doi.org/10.1016/S0012-821X\(03\)00292-9](https://doi.org/10.1016/S0012-821X(03)00292-9).
- Ding, S., Xu, Y., Wang, Y., He, Y., Hou, J., Chen, L., He, J.-S., 2015. Distributions of glycerol dialkyl glycerol tetraethers in surface soils of Qinghai–Tibetan Plateau: implications of GDGT-based proxies in cold and dry regions. *Biogeosciences* 12, 481–513. <https://doi.org/10.5194/bgd-12-481-2015>.
- Ding, S., Schwab, V.F., Ueberschar, N., Roth, V.-N., Lange, M., Xu, Y., Gleixner, G., Pohnert, G., 2016. Identification of novel 7-methyl and cyclopentanyl branched glycerol dialkyl glycerol tetraethers in lake sediments. *Org. Geochem.* 102, 52–58. <https://doi.org/10.1016/j.orggeochem.2016.09.009>.
- Dirghangi, S.S., Pagani, M., Hren, M.T., Tipple, B.J., 2013. Distribution of glycerol dialkyl glycerol tetraethers in soils from two environmental transects in the USA. *Org. Geochem.* 59, 49–60. <https://doi.org/10.1016/j.orggeochem.2013.03.009>.
- Filloy, A., 1985. *Le climat de la Haute-Loire*. Editions de la Borne.
- Fleimann, D., Mudelsee, M., Burns, S.J., Bradley, R.S., Kramers, J., Matter, A., 2008. Evidence for a widespread climatic anomaly at around 9.2 ka before present. *Paleoceanography* 23, PA1102. <https://doi.org/10.1029/2007PA001519>.
- Gandouin, E., Rioual, P., Pailles, C., Brooks, S.J., Ponel, P., Guiter, F., Djamali, M., Andrieu-Ponel, V., Birks, H.J.B., Leydet, M., 2016. Environmental and climatic reconstruction of the late-glacial-Holocene transition from a lake sediment sequence in Aubrac, French Massif Central: chironomid and diatom evidence. *Paleoecogr. Palaeoclimatol. Palaeoecol.* 461, 292–309. <https://doi.org/10.1016/j.palaeo.2016.08.039>.
- Geirsdóttir, Á., Miller, G.H., Larsen, D.J., Ólafsdóttir, S., 2013. Abrupt Holocene climate transitions in the northern North Atlantic region recorded by synchronized lacustrine records in Iceland. *Quat. Sci. Rev.* 70, 48–62. <https://doi.org/10.1016/j.quascirev.2013.03.010>.
- Graham, N.E., Ammann, C.M., Fleimann, D., Cobb, K.M., Luterbacher, J., 2011. Support for global climate reorganization during the “medieval climate anomaly”. *Clim. Dyn.* 37, 1217–1245. <https://doi.org/10.1007/s00382-010-0914-z>.
- Grotes, P.M., Stuiver, M., 1997. Oxygen 18/16 variability in Greenland snow and ice with 10<sup>-3</sup> to 10<sup>5</sup>-year time resolution. *J. Geophys. Res. Oceans* 102, 26455–26470. <https://doi.org/10.1029/97JC00880>.
- Guiot, J., 1990. Methodology of the last climatic cycle reconstruction in France from pollen data. *Paleoecogr. Palaeoclimatol. Palaeoecol.* 80, 49–69. [https://doi.org/10.1016/0031-0182\(90\)90033-4](https://doi.org/10.1016/0031-0182(90)90033-4).
- Guiot, J., de Beaulieu, J.L., Cheddadi, R., David, F., Ponel, P., Reille, M., 1993. The climate in Western Europe during the last Glacial/Interglacial cycle derived from pollen and insect remains. *Paleoecogr. Palaeoclimatol. Palaeoecol.* 103, 73–93. [https://doi.org/10.1016/0031-0182\(93\)90053-L](https://doi.org/10.1016/0031-0182(93)90053-L).
- Guiot, J., Torre, F., Jolly, D., Peyron, O., Boreux, J.J., Cheddadi, R., 2000. Inverse vegetation modeling by Monte Carlo sampling to reconstruct palaeoclimates under changed precipitation seasonality and CO<sub>2</sub> conditions: application to glacial climate in Mediterranean region. *Ecol. Model.* 127, 119–140. [https://doi.org/10.1016/S0304-3800\(99\)00219-7](https://doi.org/10.1016/S0304-3800(99)00219-7).
- Guiot, J., Kaniewski, D., 2015. The Mediterranean Basin and Southern Europe in a warmer world: what can we learn from the past? *Front. Earth Sci.* 3, 28. <https://doi.org/10.3389/feart.2015.00028>.
- Guo, L., Xiong, S., Ding, Z., Jin, G., Wu, J., Ye, W., 2018. Role of the mid-Holocene environmental transition in the decline of late Neolithic cultures in the deserts of NE China. *Quat. Sci. Rev.* 190, 98–113. <https://doi.org/10.1016/j.quascirev.2018.04.017>.
- Gutiérrez, M., Gutiérrez, F., Desir, G., 2006. Considerations on the chronological and causal relationships between talus flatirons and palaeoclimatic changes in central and northeastern Spain. *Geomorphology* 73, 50–63. <https://doi.org/10.1016/j.geomorph.2005.06.006>.
- Gutiérrez-Elorza, M., Peña-Monné, J.L., 1998. Geomorphology and late Holocene climatic change in Northeastern Spain. *Geomorphology* 23, 205–217. [https://doi.org/10.1016/S0169-555X\(98\)00004-X](https://doi.org/10.1016/S0169-555X(98)00004-X).
- Hammer, Ø., Harper, D.A.T., Ryan, P.D., 2001. *PAST—palaeontological Statistics*, vol. 4. *Palaeontol. Electron.*, pp. 1–9, ver. 1.89. [http://palaeo-electronica.org/2001\\_1/past/issue1\\_01.htm](http://palaeo-electronica.org/2001_1/past/issue1_01.htm).
- Harper, K., 2017. *The Fate of Rome: Climate, Disease, and the End of an Empire*. Princeton University Press, Princeton.
- Hede, M.U., Rasmussen, P., Noe-Nygaard, N., Clarke, A.L., Vinebrooke, R.D., Olsen, J., 2010. Multiproxy evidence for terrestrial and aquatic ecosystem responses during the 8.2 ka cold event as recorded at Højby Sø, Denmark. *Quat. Res.* 73, 485–496. <https://doi.org/10.1016/j.yqres.2009.12.002>.
- Heiri, O., Ilyashuk, B., Millet, L., Samartin, S., Lotter, A.F., 2015. Stacking of discontinuous regional palaeoclimate records: chironomid-based summer temperatures from the Alpine region. *Holocene* 25, 137–149. <https://doi.org/10.1177/0959683614556382>.
- Hodell, D.A., Brenner, M., Curtis, J.H., Guilderson, T., 2001. Solar forcing of drought frequency in the Maya lowlands. *Science* 292, 1367–1370. <https://doi.org/10.1126/science.1057759>.
- Hoek, W.Z., Bos, J.A.A., 2007. Early Holocene climate oscillations—causes and consequences. *Quat. Sci. Rev.* 26, 1901–1906. <https://doi.org/10.1016/j.quascirev.2007.06.008>.
- Holtvoeth, J., Vogel, H., Valsecchi, V., Lindhorst, K., Schouten, S., Wagner, B., Wolff, G.A., 2017. Linear and non-linear responses of vegetation and soils to glacial-interglacial climate change in a Mediterranean refuge. *Sci. Rep.* 7, 8121. <https://doi.org/10.1038/s41598-017-08101-y>.
- Holzhauser, H., Magny, M., Zumbühl, H.J., 2005. Glacier and lake-level variations in west-central Europe over the last 3500 years. *Holocene* 15, 789–801. <https://doi.org/10.1191/0959683605hl853ra>.
- Hopmans, E.C., Weijers, J.W., Schefuß, E., Herfort, L., Sinninghe Damsté, J.S., Schouten, S., 2004. A novel proxy for terrestrial organic matter in sediments based on branched and isoprenoid tetraether lipids. *Earth Planet. Sci. Lett.* 224, 107–116. <https://doi.org/10.1016/j.epsl.2004.05.012>.
- Hopmans, E.C., Schouten, S., Sinninghe Damsté, J.S., 2016. The effect of improved chromatography on GDGT-based palaeoproxies. *Org. Geochem.* 93, 1–6. <https://doi.org/10.1016/j.orggeochem.2015.12.006>.
- Hou, J., Li, C.-G., Lee, S., 2019. The temperature record of the Holocene: progress and controversies. *Sci. Bull.* 64, 565–566. <https://doi.org/10.1016/j.scib.2019.02.012>.
- Huguet, C., Hopmans, E.C., Febo-Ayala, W., Thompson, D.H., Sinninghe Damsté, J.S., Schouten, S., 2006. An improved method to determine the absolute abundance of glycerol dibiphytanyl glycerol tetraether lipids. *Org. Geochem.* 37, 1036–1041. <https://doi.org/10.1016/j.orggeochem.2006.05.008>.
- Huguet, A., Fosse, C., Laggoun-Défarge, F., Toussaint, M.-L., Derenne, S., 2010. Occurrence and distribution of glycerol dialkyl glycerol tetraethers in a French peat bog. *Org. Geochem.* 41, 559–572. <https://doi.org/10.1016/j.orggeochem.2010.02.015>.
- Huguet, A., Fosse, C., Laggoun-Défarge, F., Delarue, F., Derenne, S., 2013. Effects of a short-term experimental microclimate warming on the abundance and distribution of branched GDGTs in a French peatland. *Geochim. Cosmochim. Acta* 105, 294–315. <https://doi.org/10.1016/j.gca.2012.11.037>.
- Ilyashuk, E.A., Koinig, K.A., Heiri, O., Ilyashuk, B.P., Psenner, R., 2011. Holocene temperature variations at a high-altitude site in the Eastern Alps: a chironomid record from Schwarzzsee ob Sölden, Austria. *Quat. Sci. Rev.* 30, 176–191. <https://doi.org/10.1016/j.quascirev.2010.10.008>.
- Jansen, E., Overpeck, J., Briffa, K.R., Duplessy, J.C., Joos, F., Masson-Delmotte, V., Olago, D., Otto-Bliesner, B., Peltier, W.R., Rahmstorf, S., Ramesh, D., Raynaud, D., Rind, D., Solomina, O., Villalba, R., Zhang, D., 2007. *Paleoclimate*. In: Solomon, S., Qin, D., Manning, M., Chen, Z., Marquis, M., Averyt, K.B., Tignor, M., Miller, H.L. (Eds.), *Climate Change 2007: The Physical Science Basis; Contribution of Working Group I to the Fourth Assessment Report of the Intergovernmental Panel on Climate Change*. Cambridge University Press, Cambridge and New York.
- Jansen, E., Andersson, C., Moros, M., Nisancioglu, K.H., Nyland, B.F., Telford, R.J., 2008. The early to mid-Holocene thermal optimum in the North Atlantic. In: Battarbee, R.W., Binney, H.A. (Eds.), *Natural Climate Variability and Global Warming: A Holocene Perspective*. Wiley–Blackwell, pp. 123–137. <https://doi.org/10.1002/9781444300932.ch5>.
- Jorin, U.E., Stocker, T.F., Schlüchter, C., 2006. Multicentury glacier fluctuations in the Swiss Alps during the Holocene. *Holocene* 16, 697–704. <https://doi.org/10.1016/j.quascirev.2010.10.008>.

- 10.1191/0959683606hl964rp.
- Johnsen, S.J., Clausen, H.B., Dansgaard, W., Fuhrer, K., Gundestrup, N., Hammer, C.U., Iversen, P., Jouzel, J., Stauffer, B., 1992. Irregular glacial interstadials recorded in a new Greenland ice core. *Nature* 359, 311–313. <https://doi.org/10.1038/359311a0>.
- Kaiser, J., Schouten, S., Kilian, R., Arz, H.W., Lamy, F., Sinninghe Damsté, J.S., 2015. Isoprenoid and branched GDGT-based proxies for surface sediments from marine, fjord and lake environments in Chile. *Org. Geochem.* 89–90, 117–127. <https://doi.org/10.1016/j.orggeochem.2015.10.007>.
- Kaufman, D.S., Ager, T.A., Anderson, N.J., Anderson, P.M., Andrews, J.T., Bartlein, P.J., Brubaker, L.B., Coats, L.L., Cwynar, L.C., Duvall, M.L., 2004. Holocene thermal maximum in the western Arctic (0–180 W). *Quat. Sci. Rev.* 23, 529–560. <https://doi.org/10.1016/j.quascirev.2003.09.007>.
- Kluge, T., Affek, H.P., Marx, T., Aeschbach-Hertig, W., Riechelmann, D.F.C., Scholz, D., Riechelmann, S., Immenhauser, A., Richter, D.K., Fohlmeister, J., 2013. Reconstruction of drip-water  $\delta^{18}\text{O}$  based on calcite oxygen and clumped isotopes of speleothems from Bunker Cave (Germany). *Clim. Past* 9, 377–391. <https://doi.org/10.5194/cp-9-377-2013>.
- Kobashi, T., Severinghaus, J.P., Newman, E.J., Barnola, J.-M., Grachev, A.M., 2007. Precise timing and characterization of abrupt climate change 8200 years ago from air trapped in polar ice. *Quat. Sci. Rev.* 26, 1212–1222. <https://doi.org/10.1016/j.quascirev.2007.01.009>.
- Kobashi, T., Menviel, L., Jeltsch-Thömmes, A., Vinther, B.M., Box, J.E., Muscheler, R., Nakaegawa, T., Pfister, P.L., Döring, M., Leuenberger, M., Wanner, H., Ohmura, A., 2017. Volcanic influence on centennial to millennial Holocene Greenland temperature change. *Sci. Rep.* 7, 1441. <https://doi.org/10.1038/s41598-017-01451-7>.
- Landscheidt, T., 1987. Long-range forecasts of solar cycles and climate change. In: Rampino, M., Sanders, J., Newman, W., Königsson, L. (Eds.), *Climate History, Periodicity, and Predictability*. van Nostrand Reinhold, New York, p. 445.
- Laskar, J., Robutel, P., Joutel, F., Gastineau, M., Correia, A.C.M., Levrard, B., 2004. A long-term numerical solution for the insolation quantities of the Earth. *Astron. Astrophys.* 428, 261–285. <https://doi.org/10.1051/0004-6361:20041335>.
- Lauterbach, S., Brauer, A., Andersen, N., Danielopol, D.L., Dulski, P., Hüls, M., Milecka, K., Namiotko, T., Obremaska, M., Von Grafenstein, U., Declakes Participants, 2011. Environmental responses to Lateglacial climatic fluctuations recorded in the sediments of pre-Alpine Lake Mondsee (northeastern Alps). *J. Quat. Sci.* 26, 253–267. <https://doi.org/10.1002/jqs.1448>.
- Leduc, G., Schneider, R., Kim, J.-H., Lohmann, G., 2010. Holocene and Eemian sea surface temperature trends as revealed by alkenone and Mg/Ca paleothermometry. *Quat. Sci. Rev.* 29, 989–1004. <https://doi.org/10.1016/j.quascirev.2010.01.004>.
- Lei, Y., Yang, H., Dang, X., Zhao, S., Xie, S., 2016. Absence of a significant bias towards summer temperature in branched tetraether-based paleothermometer at two soil sites with contrasting temperature seasonality. *Org. Geochem.* 94, 83–94. <https://doi.org/10.1016/j.orggeochem.2016.02.003>.
- Lindén, M., Möller, P.E.R., Björck, S., Sandgren, P., 2006. Holocene shore displacement and deglaciation chronology in Norrbotten, Sweden. *Boreas* 35, 1–22. <https://doi.org/10.1111/j.1502-3885.2006.tb01109.x>.
- Liu, Y., Zhang, M., Liu, Z., Xia, Y., Huang, Y., Peng, Y., Zhu, J., 2018. A possible role of dust in resolving the Holocene temperature conundrum. *Sci. Rep.* 8, 4434. <https://doi.org/10.1038/s41598-018-22841-5>.
- Liu, Z., Zhu, J., Rosenthal, Y., Zhang, X., Otto-Bliesner, B.L., Timmermann, A., Smith, R.S., Lohmann, G., Zheng, W., Timm, O.E., 2014. The Holocene temperature conundrum. *Proc. Natl. Acad. Sci.* 111, E3501–E3505. <https://doi.org/10.1073/pnas.1407229111>.
- Loomis, S.E., Russell, J.M., Sinninghe Damsté, J.S., 2011. Distributions of branched GDGTs in soils and lake sediments from western Uganda: implications for a lacustrine paleothermometer. *Org. Geochem.* 42, 739–751. <https://doi.org/10.1016/j.orggeochem.2011.06.004>.
- Loomis, S.E., Russell, J.M., Ladd, B., Street-Perrott, F.A., Sinninghe Damsté, J.S., 2012. Calibration and application of the branched GDGT temperature proxy on East African lake sediments. *Earth Planet. Sci. Lett.* 357–358, 277–288. <https://doi.org/10.1016/j.epsl.2012.09.031>.
- Loomis, S.E., Russell, J.M., Heurich, A.M., D'Andrea, W.J., Sinninghe Damsté, J.S., 2014. Seasonal variability of branched glycerol dialkyl glycerol tetraethers (brGDGTs) in a temperate lake system. *Geochim. Cosmochim. Acta* 144, 173–187. <https://doi.org/10.1016/j.gca.2014.08.027>.
- Lüning, S., Galka, M., Vahrenholt, F., 2017. Warming and cooling: the medieval climate anomaly in Africa and Arabia. *Paleoceanography* 32, 1219–1235. <https://doi.org/10.1002/2017PA003237>.
- Magny, M., 2004. Holocene climate variability as reflected by mid-European lake-level fluctuations and its probable impact on prehistoric human settlements. *Quat. Int.* 113, 65–79. [https://doi.org/10.1016/S1040-6182\(03\)00080-6](https://doi.org/10.1016/S1040-6182(03)00080-6).
- Magny, M., Haas, J.N., 2004. A major widespread climatic change around 5300 cal. yr BP at the time of the Alpine Iceman. *J. Quat. Sci.* 19, 423–430. <https://doi.org/10.1002/jqs.850>.
- Magny, M., Leuzinger, U., Bortenschlager, S., Haas, J.N., 2006. Tripartite climate reversal in Central Europe 5600–5300 years ago. *Quat. Res.* 65, 3–19. <https://doi.org/10.1016/j.yqres.2005.06.009>.
- Magny, M., Comboudieu-Nebout, N., Beaulieu, J.L. de, Bout-Roumazeilles, V., Colombarelli, D., Desprat, S., Francke, A., Joannin, S., Ortu, E., Peyron, O., Revel, M., Sadori, L., Siani, G., Sicre, M.A., Samartin, S., Simonneau, A., Tinner, W., Vannièr, B., Wagner, B., Zanchetta, C., Anselmetti, F., Brugiapaglia, E., Chapron, E., Debret, M., Desmet, M., Didier, J., Essallami, L., Galop, D., Gilli, A., Haas, J.N., Kallel, N., Millet, L., Stock, A., Turon, J.L., Wirth, S., 2013. North-south palaeohydrological contrasts in the central Mediterranean during the Holocene: tentative synthesis and working hypotheses. *Clim. Past* 9, 2043–2071. <https://doi.org/10.5194/cp-9-2043-2013>.
- Mann, M.E., Zhang, Z., Rutherford, S., Bradley, R.S., Hughes, M.K., Shindell, D., Ammann, C., Caluvelgi, G., Ni, F., 2009. Global signatures and dynamical origins of the little ice age and medieval climate anomaly. *Science* 326, 1256–1260. <https://doi.org/10.1126/science.1177303>.
- Marcott, S.A., Shakun, J.D., Clark, P.U., Mix, A.C., 2013. A reconstruction of regional and global temperature for the past 11,300 years. *Science* 339, 1198–1201. <https://doi.org/10.1126/science.1228026>.
- Marsicek, J., Shuman, B.N., Bartlein, P.J., Shafer, S.L., Brewer, S., 2018. Reconciling divergent trends and millennial variations in Holocene temperatures. *Nature* 554, 92–96. <https://doi.org/10.1038/nature25464>.
- Martin, C., Ménot, G., Thouveny, N., Davtian, N., Andrieu-Ponel, V., Reille, M., Bard, E., 2019. Impact of human activities and vegetation changes on the tetraether sources in Lake St Front (Massif Central, France). *Org. Geochem.* 135, 38–52. <https://doi.org/10.1016/j.orggeochem.2019.06.005>.
- Martin-Puertas, C., Matthes, K., Brauer, A., Muscheler, R., Hansen, F., Petrick, C., Aldahan, A., Possnert, G., van Geel, B., 2012. Regional atmospheric circulation shifts induced by a grand solar minimum. *Nat. Geosci.* 5, 397–401. <https://doi.org/10.1038/ngeo1460>.
- Martrat, B., Jimenez-Amat, P., Zahn, R., Grimalt, J.O., 2014. Similarities and dissimilarities between the last two deglaciations and interglaciations in the North Atlantic region. *Quat. Sci. Rev.* 99, 122–134. <https://doi.org/10.1016/j.quascirev.2014.06.016>.
- Matero, I.S.O., Gregoire, L.J., Ivanovic, R.F., Tindall, J.C., Haywood, A.M., 2017. The 8.2 ka cooling event caused by Laurentide ice saddle collapse. *Earth Planet. Sci. Lett.* 473, 205–214. <https://doi.org/10.1016/j.epsl.2017.06.011>.
- Mauri, A., Davis, B.A.S., Collins, P.M., Kaplan, J.O., 2014. The influence of atmospheric circulation on the mid-Holocene climate of Europe: a data-model comparison. *Clim. Past* 10, 1925–1938. <https://doi.org/10.5194/cp-10-1925-2014>.
- Mauri, A., Davis, B.A.S., Collins, P.M., Kaplan, J.O., 2015. The climate of Europe during the Holocene: a gridded pollen-based reconstruction and its multi-proxy evaluation. *Quat. Sci. Rev.* 112, 109–127. <https://doi.org/10.1016/j.quascirev.2015.01.013>.
- Mayer, B., Schwark, L., 1999. A 15,000-year stable isotope record from sediments of Lake Steisslingen, Southwest Germany. *Chem. Geol.* 161, 315–337. [https://doi.org/10.1016/S0009-2541\(99\)00093-5](https://doi.org/10.1016/S0009-2541(99)00093-5).
- Mayewski, P.A., Rohling, E.E., Stager, J.C., Karlén, W., Maasch, K.A., Meeker, L.D., Meyerson, E.A., Gasse, F., van Kereveld, S., Holmgren, K., 2004. Holocene climate variability. *Quat. Res.* 62, 243–255. <https://doi.org/10.1016/j.yqres.2004.07.001>.
- McDermott, F., Frisia, S., Huang, Y., Longinelli, A., Spiro, B., Heaton, T.H., Hawkesworth, C.J., Borsato, A., Keppens, E., Fairchild, I.J., 1999. Holocene climate variability in Europe: evidence from  $\delta^{18}\text{O}$ , textural and extension-rate variations in three speleothems. *Quat. Sci. Rev.* 18, 1021–1038. [https://doi.org/10.1016/S0277-3791\(98\)00107-3](https://doi.org/10.1016/S0277-3791(98)00107-3).
- Menges, J., Huguet, C., Alcañiz, J.M., Fietz, S., Sachse, D., Rosell-Melé, A., 2014. Influence of water availability in the distributions of branched glycerol dialkyl glycerol tetraether in soils of the Iberian Peninsula. *Biogeosciences* 11, 2571–2581. <https://doi.org/10.5194/bg-11-2571-2014>.
- Ménot, G., Bard, E., 2012. A precise search for drastic temperature shifts of the past 40,000 years in southeastern Europe. *Paleoceanography* 27, PA2210. <https://doi.org/10.1029/2012PA002291>.
- Mercuri, A.M., Sadori, L., Uzquiano Ollero, P., 2011. Mediterranean and north-African cultural adaptations to mid-Holocene environmental and climatic changes. *Holocene* 21, 189–206. <https://doi.org/10.1177/0959683610377532>.
- Mergoil, J., 1987. *Aperçu géologique du Velay*. Doc. CERLAT 1, 17–22.
- Mergoil, J., Boivin, P., Blès, J.L., Cantagrel, J.M., Turland, M., 1993. *Le Velay. Son volcanisme form.* Assoc. Geol. Fr. 3, 96.
- Meyer, V.D., Heffer, J., Lohmann, G., Max, L., Tiedemann, R., Mollenhauer, G., 2017. Summer temperature evolution on the Kamchatka peninsula, Russian far East, during the past 20 000 years. *Clim. Past* 13, 359–377. <https://doi.org/10.5194/cp-13-359-2017>.
- Miller, D.R., Habicht, M.H., Keisling, B.A., Castañeda, I.S., Bradley, R.S., 2018. A 900-year New England temperature reconstruction from in situ seasonally produced branched glycerol dialkyl glycerol tetraethers (brGDGTs). *Clim. Past* 14, 1653–1667. <https://doi.org/10.5194/cp-14-1653-2018>.
- Montade, V., Peyron, O., Favier, C., Francois, J.P., Haberle, S.G., 2019. A pollen-climate calibration from western Patagonia for palaeoclimatic reconstructions. *J. Quat. Sci.* 34, 76–86. <https://doi.org/10.1002/jqs.3082>.
- Moossen, H., Bendle, J., Seki, O., Quillmann, U., Kawamura, K., 2015. North Atlantic Holocene climate evolution recorded by high-resolution terrestrial and marine biomarker records. *Quat. Sci. Rev.* 129, 111–127. <https://doi.org/10.1016/j.quascirev.2015.01.013>.
- Moreno, A., Svensson, A., Brooks, S.J., Connor, S., Engels, S., Fletcher, W., Genty, D., Heiri, O., Labuhn, I., Perçoiu, A., Peyron, O., Sadori, L., Valero-Garcés, B., Wulf, S., Zanchetta, G., 2014. Data contributors. A compilation of Western European terrestrial records 60–8 ka BP: towards an understanding of latitudinal climatic gradients. *Quat. Sci. Rev.* 106, 167–185. <https://doi.org/10.1016/j.quascirev.2014.06.030>.
- Naafs, B.D.A., Gallego-Sala, A.V., Inglis, G.N., Pancost, R.D., 2017. Refining the global branched glycerol dialkyl glycerol tetraether (brGDGT) soil temperature calibration. *Org. Geochem.* 106, 48–56. <https://doi.org/10.1016/j.orggeochem.2017.01.009>.
- Nicolussi, K., Patzelt, G., 2000. Untersuchungen zur holozänen



- Gletscherentwicklung von Pasterze und Gepatschferner (Ostalpen). *Z. Für Gletscherkunde Glazialgeol.* 36, 1–87.
- Niemann, H., Stadnitskaia, A., Wirth, S.B., Gilli, A., Anselmetti, F.S., Sinninghe Damsté, J.S., Schouten, S., Hopmans, E.C., Lehmann, M.F., 2012. Bacterial GDGTs in Holocene sediments and catchment soils of a high Alpine lake: application of the MBT/CBT-paleothermometer. *Clim. Past* 8, 889–906. <https://doi.org/10.5194/cp-8-889-2012>.
- Nieto-Moreno, V., Rohrmann, A., van der Meer, M.T.J., Sinninghe Damsté, J.S., Sachse, D., Tofelde, S., Niedermeyer, E.M., Strecker, M.R., Mulch, A., 2016. Elevation-dependent changes in n-alkane  $\delta D$  and soil GDGTs across the south central Andes. *Earth Planet. Sci. Lett.* 453, 234–242. <https://doi.org/10.1016/j.epsl.2016.07.049>.
- Niggemann, S., Mangini, A., Richter, D.K., Wurth, G., 2003. A paleoclimate record of the last 17,600 years in stalagmites from the B7 cave, Sauerland, Germany. *Quat. Sci. Rev.* 22, 555–567. [https://doi.org/10.1016/S0277-3791\(02\)00143-9](https://doi.org/10.1016/S0277-3791(02)00143-9).
- Ning, D., Zhang, E., Shulmeister, J., Chang, J., Sun, W., Ni, Z., 2019. Holocene mean annual air temperature (MAAT) reconstruction based on branched glycerol dialkyl glycerol tetraethers from Lake Ximenglongtan, southwestern China. *Org. Geochem.* 133, 65–76. <https://doi.org/10.1016/j.orggeochem.2019.05.003>.
- North Greenland Ice Core Project Members, Andersen, K.K., Azuma, N., Barnola, J.-M., Bigler, M., Biscaye, P., Caillon, N., Chappellaz, J., Clausen, H.B., Dahl-Jensen, D., Fischer, H., Flückiger, J., Fritzsche, D., Fujii, Y., Goto-Azuma, K., Grönvold, K., Gundestrup, N.S., Hansson, M., Huber, C., Hvidberg, C.S., Johnsen, S.J., Jonsell, U., Jouzel, J., Kipfstuhl, S., Landais, A., Leuenberger, M., Lorrain, R., Masson-Delmotte, V., Miller, H., Motoyama, H., Narita, H., Popp, T., Rasmussen, S.O., Raynaud, D., Rothlisberger, R., Ruth, U., Samyn, D., Schwander, J., Shoji, H., Siggard-Andersen, M.-L., Steffensen, J.P., Stocker, T., Sveinbjörnsdóttir, A.E., Svensson, A., Takata, M., Tison, J.-L., Thorsteinsson, T., Watanabe, O., Wilhelms, F., White, J.W.C., 2004. High-resolution record of Northern Hemisphere climate extending into the last interglacial period. *Nature* 431, 147–151. <https://doi.org/10.1038/nature02805>.
- Overpeck, J.T., Webb, T., Prentice, I.C., 1985. Quantitative interpretation of fossil pollen spectra: dissimilarity coefficients and the method of modern analogs. *Quat. Res.* 23, 87–108. [https://doi.org/10.1016/0033-5894\(85\)90074-2](https://doi.org/10.1016/0033-5894(85)90074-2).
- PAGES 2k Consortium, Ahmed, M., Anchukaitis, K.J., Asrat, A., Borgaonkar, H.P., Braid, M., Buckley, B.M., Büntgen, U., Chase, B.M., Christie, D.A., Cook, E.R., Curran, M.A.J., Diaz, H.F., Esper, J., Fan, Z.-X., Gaire, N.P., Ge, Q., Gergis, J., González-Rouco, J.F., Goosse, H., Grab, S.W., Graham, N., Graham, R., Grosjean, M., Hanhijärvi, S.T., Kaufman, D.S., Kiefer, T., Kimura, K., Korhola, A.A., Krusic, P.J., Lara, A., Lézine, A.-M., Ljungqvist, F.C., Lorrey, A.M., Luterbacher, J., Masson-Delmotte, V., McCarroll, D., McConnell, J.R., McKay, N.P., Morales, M.S., Moy, A.D., Mulvaney, R., Mundo, I.A., Nakatsuka, T., Nash, D.J., Neukom, R., Nicholson, S.E., Oerter, H., Palmer, J.G., Phipps, S.J., Prieto, M.R., Rivera, A., Sano, M., Severi, M., Shanahan, T.M., Shao, X., Shi, F., Sigl, M., Smerdon, J.E., Solomina, O.N., Steig, E.J., Stenni, B., Thamban, M., Trouet, V., Turney, C.S.M., Umer, M., Ommen, T., van, Verschuren, D., Viau, A.E., Villalba, R., Vinther, B.M., Gunten, L. von, Wagner, S., Wahl, E.R., Wanner, H., Werner, J.P., White, J.W.C., Yasue, K., Zorita, E., 2013. Continental-scale temperature variability during the past two millennia. *Nat. Geosci.* 6, 339–346. <https://doi.org/10.1038/ngeo1797>.
- Panizza, M., 1985. Schemi cronologici del Quaternario. *Geogr. Fis. Dinam. Quat* 8, 44–48.
- Pei, Q., Zhang, D.D., Li, J., Lee, H.F., 2017. Proxy-based northern hemisphere temperature reconstruction for the mid-to-late Holocene. *Theor. Appl. Climatol.* 130, 1043–1053. <https://doi.org/10.1007/s00704-016-1932-5>.
- Peltier, W.R., 2004. Global glacial isostasy and the surface of the ice-age Earth: the ICE-5G (VM2) model and GRACE. *Annu. Rev. Earth Planet Sci.* 32, 111–149. <https://doi.org/10.1146/annurev.earth.32.082503.144359>.
- Peterse, F., Nicol, G.W., Schouten, S., Sinninghe Damsté, J.S., 2010. Influence of soil pH on the abundance and distribution of core and intact polar lipid-derived branched GDGTs in soil. *Org. Geochem.* 41, 1171–1175. <https://doi.org/10.1016/j.orggeochem.2010.07.004>.
- Peterse, F., van der Meer, J., Schouten, S., Weijers, J.W., Fierer, N., Jackson, R.B., Kim, J.-H., Sinninghe Damsté, J.S., 2012. Revised calibration of the MBT–CBT paleotemperature proxy based on branched tetraether membrane lipids in surface soils. *Geochem. Cosmochim. Acta* 96, 215–229. <https://doi.org/10.1016/j.gca.2012.08.011>.
- Peterse, F., Vonk, J.E., Holmes, R.M., Giosan, L., Zimov, N., Eglinton, T.I., 2014. Branched glycerol dialkyl glycerol tetraethers in Arctic lake sediments: sources and implications for paleothermometry at high latitudes. *J. Geophys. Res. Biogeosci.* 119, 1738–1754. <https://doi.org/10.1002/2014JG002639>.
- Peyron, O., Bégoet, C., Brewer, S., Heiri, O., Magny, M., Millet, L., Ruffaldi, P., Van Campo, E., Yu, G., 2005. Late-Glacial climatic changes in Eastern France (Lake Lautrey) from pollen, lake-levels, and chironomids. *Quat. Res.* 64, 197–211. <https://doi.org/10.1016/j.yqres.2005.01.006>.
- Peyron, O., Goring, S., Dormoy, I., Kotthoff, U., Pross, J., De Beaulieu, J.-L., Drescher-Schneider, R., Vannié, B., Magny, M., 2011. Holocene seasonality changes in the central Mediterranean region reconstructed from the pollen sequences of Lake Accesa (Italy) and Tenaghi Philippon (Greece). *Holocene* 21, 131–146. <https://doi.org/10.1177/0959683610384162>.
- Peyron, O., Magny, M., Goring, S., Joannin, S., De Beaulieu, J.-L., Bruggiapaglia, E., Sadori, L., Garfi, G., Kouli, K., Ioakim, C., Combourieu Nebout, N., 2013. Contrasting patterns of climatic changes during the Holocene across the Italian Peninsula reconstructed from pollen data. *Clim. Past* 9, 1233–1252. <https://doi.org/10.5194/cp-9-1233-2013>.
- Peyron, O., Combourieu-Nebout, N., Brayshaw, D., Goring, S., Andrieu-Ponel, V., Desprat, S., Fletcher, W., Gambin, B., Ioakim, C., Joannin, S., 2017. Precipitation changes in the Mediterranean basin during the Holocene from terrestrial and marine pollen records: a model-data comparison. *Clim. Past* 13, 249–265. <https://doi.org/10.5194/cp-13-249-2017>.
- Ponel, P., Guiter, F., Gandouin, E., Pailles, C., Rioual, P., Djamali, M., Andrieu-Ponel, V., Leydet, M., Van der Putten, N., de Beaulieu, J.-L., 2016. Novel insights from coleopteran and pollen evidence into the Lateglacial/Holocene transition in Aubrac, French Massif Central. *Palaeogeogr. Palaeoclimatol. Palaeoecol.* 463, 83–102. <https://doi.org/10.1016/j.palaeo.2016.09.020>.
- Prentice, I.C., Parsons, R.W., 1983. Maximum likelihood linear calibration of pollen spectra in terms of forest composition. *Biometrics* 39, 1051–1057. <https://doi.org/10.2307/2531338>.
- Prentice, I.C., Cramer, W., Harrison, S.P., Leemans, R., Monserud, R.A., Solomon, A.M., 1992. Special Paper: a global biome model based on plant Physiology and dominance, soil Properties and climate. *J. Biogeogr.* 19, 117–134. <https://doi.org/10.2307/2845499>.
- Quillmann, U., Marchitto, T.M., Jennings, A.E., Andrews, J.T., Friestad, B.F., 2012. Cooling and freshening at 8.2 ka on the NW Iceland Shelf recorded in paired  $\delta^{18}O$  and Mg/Ca measurements of the benthic foraminifer *Cibicides lobatulus*. *Quat. Res.* 78, 528–539. <https://doi.org/10.1016/j.yqres.2012.08.003>.
- Rasmussen, S.O., Vinther, B.M., Clausen, H.B., Andersen, K.K., 2007. Early Holocene climate oscillations recorded in three Greenland ice cores. *Quat. Sci. Rev.* 26, 1907–1914. <https://doi.org/10.1016/j.quascirev.2007.06.015>.
- Rasmussen, S.O., Bigler, M., Blockley, S.P., Blunier, T., Buchardt, S.L., Clausen, H.B., Cvijanovic, I., Dahl-Jensen, D., Johnsen, S.J., Fischer, H., 2014. A stratigraphic framework for abrupt climatic changes during the Last Glacial period based on three synchronized Greenland ice-core records: refining and extending the INTIMATE event stratigraphy. *Quat. Sci. Rev.* 106, 14–28. <https://doi.org/10.1016/j.quascirev.2014.09.007>.
- Rehfeld, K., Trachsel, M., Telford, R.J., Laepple, T., 2016. Assessing performance and seasonal bias of pollen-based climate reconstructions in a perfect model world. *Clim. Past* 12, 2255–2270. <https://doi.org/10.5194/cp-12-2255-2016>.
- Rehfeld, K., Münch, T., Ho, S.L., Laepple, T., 2018. Global patterns of declining temperature variability from the last glacial maximum to the Holocene. *Nature* 554, 356–359. <https://doi.org/10.1038/nature25454>.
- Reille, M., de Beaulieu, J.L., 1988. History of the Würm and Holocene vegetation in western Velay (Massif Central, France): a comparison of pollen analysis from three corings at Lac du Bouchet. *Rev. Palaeobot. Palynol.* 54, 233–248. [https://doi.org/10.1016/0034-6667\(88\)90016-4](https://doi.org/10.1016/0034-6667(88)90016-4).
- Reille, M., de Beaulieu, J.L., 1990. Pollen analysis of a long upper Pleistocene continental sequence in a Velay maar (Massif Central, France). *Palaeogeogr. Palaeoclimatol. Palaeoecol.* 80, 35–48. [https://doi.org/10.1016/0031-0182\(90\)90032-3](https://doi.org/10.1016/0031-0182(90)90032-3).
- Reille, M., Pons, A., de Beaulieu, J.-L., 1992. Late and post-glacial vegetation, climate and human action in the French Massif Central. *Cah. Micropaleontol.* 7 (1/2), 93–106.
- Renssen, H., Seppä, H., Heiri, O., Roche, D.M., Goosse, H., Fichet, T., 2009. The spatial and temporal complexity of the Holocene thermal maximum. *Nat. Geosci.* 2, 411–414. <https://doi.org/10.1038/ngeo513>.
- Renssen, H., Seppä, H., Crosta, X., Goosse, H., Roche, D.M., 2012. Global characterization of the Holocene thermal maximum. *Quat. Sci. Rev.* 48, 7–19. <https://doi.org/10.1016/j.quascirev.2012.05.022>.
- Rhoujjati, A., 1995. Géochimie organique et changements environnementaux du dernier cycle climatique: étude des sédiments du lac Saint Front (Massif Central, France). Université Aix-Marseille II.
- Roberts, N., Brayshaw, D., Kuzucuoglu, C., Perez, R., Sadori, L., 2011. The mid-Holocene climatic transition in the Mediterranean: causes and consequences. *Holocene* 21, 3–13. <https://doi.org/10.1177/0959683610388058>.
- Rosenthal, Y., Linsley, B.K., Oppo, D.W., 2013. Pacific Ocean heat content during the past 10,000 years. *Science* 342, 617–621. <https://doi.org/10.1126/science.1240837>.
- Rosenthal, Y., Kalansky, J., Morley, A., Linsley, B., 2017. A paleo-perspective on ocean heat content: lessons from the Holocene and Common Era. *Quat. Sci. Rev.* 155, 1–12. <https://doi.org/10.1016/j.quascirev.2016.10.017>.
- Rueda, G., Rosell-Melé, A., Escala, M., Gyllencreutz, R., Backman, J., 2009. Comparison of instrumental and GDGT-based estimates of sea surface and air temperatures from the Skagerrak. *Org. Geochem.* 40, 287–291. <https://doi.org/10.1016/j.orggeochem.2008.10.012>.
- Russell, J.M., Hopmans, E.C., Loomis, S.E., Liang, J., Sinninghe Damsté, J.S., 2018. Distributions of 5- and 6-methyl branched glycerol dialkyl glycerol tetraethers (brGDGTs) in East African lake sediment: effects of temperature, pH, and new lacustrine paleotemperature calibrations. *Org. Geochem.* 117, 56–69. <https://doi.org/10.1016/j.orggeochem.2017.12.003>.
- Salonen, J.S., Korpela, M., Williams, J.W., Luoto, M., 2019. Machine-learning based reconstructions of primary and secondary climate variables from North American and European fossil pollen data. *Sci. Rep.* 9, 1–13. <https://doi.org/10.1038/s41598-019-52293-4>.
- Samartin, S., Heiri, O., Joos, F., Renssen, H., Franke, J., Brönnimann, S., Tinner, W., 2017. Warm Mediterranean mid-Holocene summers inferred from fossil midge assemblages. *Nat. Geosci.* 10, 207–212. <https://doi.org/10.1038/ngeo2891>.
- Sanchi, L., Ménot, G., Bard, E., 2013. An automated purification method for archaeal and bacterial tetraethers in soils and sediments. *Org. Geochem.* 54, 83–90. <https://doi.org/10.1016/j.orggeochem.2012.10.005>.
- Sanchi, L., Ménot, G., Bard, E., 2014. Insights into continental temperatures in the northwestern Black Sea area during the Last Glacial period using branched



- tetraether lipids. *Quat. Sci. Rev.* 84, 98–108. <https://doi.org/10.1016/j.quascirev.2013.11.013>.
- Sandweiss, D.H., Maasch, K.A., Burger, R.L., Richardson III, J.B., Rollins, H.B., Clement, A., 2001. Variation in Holocene El Niño frequencies: climate records and cultural consequences in ancient Peru. *Geology* 29, 603–606. [https://doi.org/10.1130/0091-7613\(2001\)029<0603:VIHENO>2.0.CO;2](https://doi.org/10.1130/0091-7613(2001)029<0603:VIHENO>2.0.CO;2).
- Schouten, S., Hopmans, E.C., Pancost, R.D., Sinninghe Damsté, J.S., 2000. Widespread occurrence of structurally diverse tetraether membrane lipids: evidence for the ubiquitous presence of low-temperature relatives of hyperthermophiles. *Proc. Natl. Acad. Sci.* 97, 14421–14426. <https://doi.org/10.1073/pnas.97.26.14421>.
- Shanahan, T.M., Hughen, K.A., Van Mooy, B.A.S., 2013. Temperature sensitivity of branched and isoprenoid GDGTs in Arctic lakes. *Org. Geochem.* 64, 119–128. <https://doi.org/10.1016/j.orggeochem.2013.09.010>.
- Shuman, B., 2012. Patterns, processes, and impacts of abrupt climate change in a warm world: the past 11,700 years. *Wiley Interdiscipl. Rev.: Clim. Change* 3, 19–43. <https://doi.org/10.1002/wcc.152>.
- Sicre, M.-A., Jacob, J., Ezat, U., Rousse, S., Kissel, C., Yiou, P., Eiríksson, J., Knudsen, K.L., Jansen, E., Turon, J.-L., 2008. Decadal variability of sea surface temperatures off North Iceland over the last 2000 years. *Earth Planet. Sci. Lett.* 268, 137–142. <https://doi.org/10.1016/j.epsl.2008.01.011>.
- Sinninghe Damsté, J.S., 2016. Spatial heterogeneity of sources of branched tetraethers in shelf systems: the geochemistry of tetraethers in the Berau River delta (Kalimantan, Indonesia). *Geochem. Cosmochim. Acta* 186, 13–31. <https://doi.org/10.1016/j.gca.2016.04.033>.
- Sinninghe Damsté, J.S., Ossebaer, J., Schouten, S., Verschuren, D., 2008. Altitudinal shifts in the branched tetraether lipid distribution in soil from Mt. Kilimanjaro (Tanzania): implications for the MBT/CBT continental palaeothermometer. *Org. Geochem.* 39, 1072–1076. <https://doi.org/10.1016/j.orggeochem.2007.11.011>.
- Sinninghe Damsté, J.S., Rijpstra, W.I.C., Hopmans, E.C., Weijers, J.W.H., Foesel, B.U., Overmann, J., Dedysh, S.N., 2011. 13,16-Dimethyl octacosanedioic acid (iso-diabolic acid), a common membrane-spanning lipid of Acidobacteria subdivisions 1 and 3. *Appl. Environ. Microbiol.* 77, 4147–4154. <https://doi.org/10.1128/AEM.00466-11>.
- Sinninghe Damsté, J.S., Ossebaer, J., Schouten, S., Verschuren, D., 2012. Distribution of tetraether lipids in the 25-ka sedimentary record of Lake Challa: extracting reliable TEX<sub>86</sub> and MBT/CBT palaeotemperatures from an equatorial African lake. *Quat. Sci. Rev.* 50, 43–54. <https://doi.org/10.1016/j.quascirev.2012.07.001>.
- Sinninghe Damsté, J.S., Rijpstra, W.I.C., Hopmans, E.C., Foesel, B.U., Wüst, P.K., Overmann, J., Tank, M., Bryant, D.A., Dunfield, P.F., Houghton, K., Stott, M.B., 2014. Ether- and ester-bound iso-diabolic acid and other lipids in members of Acidobacteria subdivision 4. *Appl. Environ. Microbiol.* 80, 5207–5218. <https://doi.org/10.1128/AEM.01066-14>.
- Sinninghe Damsté, J.S., Rijpstra, W.I.C., Foesel, B.U., Huber, K.J., Overmann, J., Nakagawa, S., Kim, J.J., Dunfield, P.F., Dedysh, S.N., Villanueva, L., 2018. An overview of the occurrence of ether- and ester-linked iso-diabolic acid membrane lipids in microbial cultures of the Acidobacteria: implications for brGDGT paleoproxies for temperature and pH. *Org. Geochem.* 124, 63–76. <https://doi.org/10.1016/j.orggeochem.2018.07.006>.
- Sirocko, F., Sarnthein, M., Erlenkeuser, H., Lange, H., Arnold, M., Duplessy, J.C., 1993. Century-scale events in monsoonal climate over the past 24,000 years. *Nature* 364, 322–324. <https://doi.org/10.1038/364322a0>.
- Sobrinho, R.L., Bernardes, M.C., Abril, G., Kim, J.-H., Zell, C.I., Mortillaro, J.-M., Meziane, T., Moreira-Turcq, P., Sinninghe Damsté, J., 2016. Spatial and seasonal contrasts of sedimentary organic matter in floodplain lakes of the central Amazon basin. *Biogeosciences* 13, 467–482. <https://doi.org/10.5194/bg-13-467-2016>.
- Solomina, O.N., Bradley, R.S., Hodgson, D.A., Ivy-Ochs, S., Jomelli, V., Mackintosh, A.N., Nesje, A., Owen, L.A., Wanner, H., Wiles, G.C., Young, N.E., 2015. Holocene glacier fluctuations. *Quat. Sci. Rev.* 111, 9–34. <https://doi.org/10.1016/j.quascirev.2014.11.018>.
- Stanley, J.-D., Krom, M.D., Cliff, R.A., Woodward, J.C., 2003. Short contribution: Nile flow failure at the end of the Old Kingdom, Egypt: strontium isotopic and petrological evidence. *Geoarchaeology* 18, 395–402. <https://doi.org/10.1002/gea.10065>.
- Staubwasser, M., Sirocko, F., Grootes, P.M., Segl, M., 2003. Climate change at the 4.2 ka BP termination of the Indus valley civilization and Holocene south Asian monsoon variability. *Geophys. Res. Lett.* 30, 1425. <https://doi.org/10.1029/2002GL016822>.
- Staubwasser, M., Weiss, H., 2006. Holocene climate and cultural evolution in late prehistoric–early historic West Asia. *Quat. Res.* 66, 372–387. <https://doi.org/10.1016/j.yqres.2006.09.001>.
- Sun, Q., Chu, G., Liu, M., Xie, M., Li, S., Ling, Y., Wang, X., Shi, L., Jia, G., Lü, H., 2011. Distributions and temperature dependence of branched glycerol dialkyl glycerol tetraethers in recent lacustrine sediments from China and Nepal. *J. Geophys. Res.* 116, G01008. <https://doi.org/10.1029/2010JG001365>.
- Swindles, G.T., Plunkett, G., Roe, H.M., 2007. A delayed climatic response to solar forcing at 2800 cal. BP: multiproxy evidence from three Irish peatlands. *Holocene* 17, 177–182. <https://doi.org/10.1177/0959683607075830>.
- ter Braak, C.J., Juggins, S., 1993. Weighted averaging partial least squares regression (WA-PLS): an improved method for reconstructing environmental variables from species assemblages. In: *Twelfth International Diatom Symposium*. Springer, pp. 485–502. [https://doi.org/10.1007/978-94-017-3622-0\\_49](https://doi.org/10.1007/978-94-017-3622-0_49).
- Tarros, P., Carrión, J., Dorado-Valiño, M., Queiroz, P., Santos, L., Valdeolmillos-Rodríguez, A., Célio Alves, P., Brito, J.C., Cheddadi, R., 2016. Spatial climate dynamics in the Iberian peninsula since 15 000 yr BP. *Clim. Past* 12, 1137–1149. <https://doi.org/10.5194/cp-12-1137-2016>.
- Teulade, A., Mergoil, J., Boivin, A., 1991. Etudes géologiques et volcanologiques des environs du Lac du Bouchet. In: Bonifay, E. (Ed.), *Le Lac Du Bouchet (1) Environnement Naturel et Études Des Sédiments Du Dernier Cycle Climatique, Documents Du Centre d'Étude et de Recherche Sur Les Lacs, Anciens Lacs et Tourbières Du Massif Central 2*. Le Puy, pp. 63–78.
- Thomas, E.K., Clemens, S.C., Sun, Y., Huang, Y., Prell, W., Chen, G., Liu, Z., Loomis, S., 2017. Midlatitude land surface temperature impacts the timing and structure of glacial maxima. *Geophys. Res. Lett.* 44, 984–992. <https://doi.org/10.1002/2016GL071882>.
- Tierney, J.E., Russell, J.M., 2009. Distributions of branched GDGTs in a tropical lake system: implications for lacustrine application of the MBT/CBT paleoproxy. *Org. Geochem.* 40, 1032–1036. <https://doi.org/10.1016/j.orggeochem.2009.04.014>.
- Tierney, J.E., Russell, J.M., Eggermont, H., Hopmans, E.C., Verschuren, D., Sinninghe Damsté, J.S., 2010. Environmental controls on branched tetraether lipid distributions in tropical East African lake sediments. *Geochem. Cosmochim. Acta* 74, 4902–4918. <https://doi.org/10.1016/j.gca.2010.06.002>.
- Tierney, J.E., Schouten, S., Pitcher, A., Hopmans, E.C., Sinninghe Damsté, J.S., 2012. Core and intact polar glycerol dialkyl glycerol tetraethers (GDGTs) in Sand Pond, Warwick, Rhode Island (USA): insights into the origin of lacustrine GDGTs. *Geochem. Cosmochim. Acta* 77, 561–581. <https://doi.org/10.1016/j.gca.2011.10.018>.
- Trouet, V., Esper, J., Graham, N.E., Baker, A., Scourse, J.D., Frank, D.C., 2009. Persistent positive North Atlantic Oscillation mode dominated the medieval climate anomaly. *Science* 324, 78–80. <https://doi.org/10.1126/science.1166349>.
- van Geel, B., van Der Plicht, J., Kilian, M.R., Klaver, E.R., Kouwenberg, J.H.M., Renssen, H., Reynaud-Farrera, I., Waterbolk, H.T., 1997. The sharp rise of  $\delta^{14}\text{C}$  ca. 800 cal BC: possible causes, related climatic teleconnections and the impact on human environments. *Radiocarbon* 40, 535–550. <https://doi.org/10.1017/S003822200018403>.
- van Geel, B., Heusser, C.J., Renssen, H., Schuurmans, C.J., 2000. Climatic change in Chile at around 2700 BP and global evidence for solar forcing: a hypothesis. *Holocene* 10, 659–664. <https://doi.org/10.1191/09596830094908>.
- Viau, A.E., Gajewski, K., Sawada, M.C., Fines, P., 2006. Millennial-scale temperature variations in North America during the Holocene. *J. Geophys. Res. Atmos.* 111, D09102. <https://doi.org/10.1029/2005JD006031>.
- Vlag, P., Thouveny, N., Williamson, D., Andrieu, V., Icole, M., Van Velzen, A.J., 1997. The rock magnetic signal of climate change in the maar lake sequence of Lac St Front (France). *Geophys. J. Int.* 131, 724–740. <https://doi.org/10.1111/j.1365-246X.1997.tb06608.x>.
- Vollweier, N., Denis, Scholz, Christian, Mühlinghaus, Augusto, Mangini, Christoph, Spötl, 2006. A precisely dated climate record for the last 9 kyr from three high alpine stalagmites, Spannagel Cave, Austria. *Geophys. Res. Lett.* 33, L20703. <https://doi.org/10.1029/2006GL027662>.
- Wang, H., Liu, W., Zhang, C.L., Wang, Z., Wang, J., Liu, Z., Dong, H., 2012a. Distribution of glycerol dialkyl glycerol tetraethers in surface sediments of Lake Qinghai and surrounding soil. *Org. Geochem.* 47, 78–87. <https://doi.org/10.1016/j.orggeochem.2012.03.008>.
- Wang, T., Surge, D., Mithen, S., 2012b. Seasonal temperature variability of the Neoglacial (3300–2500BP) and Roman Warm Period (2500–1600BP) reconstructed from oxygen isotope ratios of limpet shells (*Patella vulgata*), Northwest Scotland. *Palaeogeogr. Palaeoclimatol. Palaeoecol.* 317–318, 104–113. <https://doi.org/10.1016/j.palaeo.2011.12.016>.
- Wang, H., Liu, W., Zhang, C.L., 2014. Dependence of the cyclization of branched tetraethers on soil moisture in alkaline soils from arid–subhumid China: implications for palaeorainfall reconstructions on the Chinese Loess Plateau. *Biogeosciences* 11, 6755–6768. <https://doi.org/10.5194/bg-11-6755-2014>.
- Wanner, H., Beer, J., Bütikofer, J., Crowley, T.J., Cubasch, U., Flückiger, J., Goosse, H., Grosjean, M., Joos, F., Kaplan, J.O., 2008. Mid- to Late Holocene climate change: an overview. *Quat. Sci. Rev.* 27, 1791–1828. <https://doi.org/10.1016/j.quascirev.2008.06.013>.
- Wanner, H., Solomina, O., Grosjean, M., Ritz, S.P., Jetel, M., 2011. Structure and origin of Holocene cold events. *Quat. Sci. Rev.* 30, 3109–3123. <https://doi.org/10.1016/j.quascirev.2011.07.010>.
- Wanner, H., Mercolli, L., Grosjean, M., Ritz, S.P., 2015. Holocene climate variability and change: a data-based review. *J. Geol. Soc.* 172, 254–263. <https://doi.org/10.1144/jgs2013-101>.
- Watson, B.L., Williams, J.W., Russell, J.M., Jackson, S.T., Shane, L., Lowell, T.V., 2018. Temperature variations in the southern Great Lakes during the last deglaciation: comparison between pollen and GDGT proxies. *Quat. Sci. Rev.* 182, 78–92. <https://doi.org/10.1016/j.quascirev.2017.12.011>.
- Wei, D., González-Sampériz, P., Gil-Romera, G., Harrison, S.P., Prentice, I.C., 2019. Climate changes in interior semi-arid Spain from the last interglacial to the late Holocene. *Clim. Past Discuss.* 1–31. <https://doi.org/10.5194/cp-2019-16>.
- Weijers, J.W., Schouten, S., Hopmans, E.C., Geenevasen, J.A., David, O.R., Coleman, J.M., Pancost, R.D., Sinninghe Damsté, J.S., 2006a. Membrane lipids of mesophilic anaerobic bacteria thriving in peats have typical archaeal traits. *Environ. Microbiol.* 8, 648–657. <https://doi.org/10.1111/j.1462-2920.2005.00941.x>.
- Weijers, J.W., Schouten, S., Spaargaren, O.C., Sinninghe Damsté, J.S., 2006b. Occurrence and distribution of tetraether membrane lipids in soils: implications for the use of the TEX<sub>86</sub> proxy and the BIT index. *Org. Geochem.* 37, 1680–1693. <https://doi.org/10.1016/j.orggeochem.2006.07.018>.
- Weijers, J.W., Schouten, S., Sluijs, A., Brinkhuis, H., Sinninghe Damsté, J.S., 2007a. Warm arctic continents during the Palaeocene–Eocene thermal maximum.

- Earth Planet. Sci. Lett. 261, 230–238. <https://doi.org/10.1016/j.epsl.2007.06.033>.
- Weijers, J.W., Schouten, S., van den Donker, J.C., Hopmans, E.C., Sinninghe Damsté, J.S., 2007b. Environmental controls on bacterial tetraether membrane lipid distribution in soils. *Geochim. Cosmochim. Acta* 71, 703–713. <https://doi.org/10.1016/j.gca.2006.10.003>.
- Weijers, J.W., Panoto, E., van Bleijswijk, J., Schouten, S., Rijpstra, W.I.C., Balk, M., Stams, A.J., Sinninghe Damsté, J.S., 2009. Constraints on the biological source(s) of the orphan branched tetraether membrane lipids. *Geomicrobiol. J.* 26, 402–414. <https://doi.org/10.1080/01490450902937293>.
- Weijers, J.W.H., Wiesenberg, G.L., Bol, R., Hopmans, E.C., Pancost, R.D., 2010. Carbon isotopic composition of branched tetraether membrane lipids in soils suggest a rapid turnover and a heterotrophic life style of their source organism(s). *Biogeosciences* 7, 2959–2973. <https://doi.org/10.5194/bg-7-2959-2010>.
- Weijers, J.W., Bernhardt, B., Peterse, F., Werne, J.P., Dungait, J.A., Schouten, S., Sinninghe Damsté, J.S., 2011. Absence of seasonal patterns in MBT–CBT indices in mid-latitude soils. *Geochim. Cosmochim. Acta* 75, 3179–3190. <https://doi.org/10.1016/j.gca.2011.03.015>.
- Weiss, H., Courty, M.-A., Wetterstrom, W., Guichard, F., Senior, L., Meadow, R., Curnow, A., 1993. The genesis and collapse of third millennium north Mesopotamian civilization. *Science* 261, 995–1004. <https://doi.org/10.1126/science.261.5124.995>.
- Weiss, H., 2012. *Seven Generations since the Fall of Akkad*. Harrassowitz Verlag, Wiesbaden.
- Xiao, W., Wang, Y., Zhou, S., Hu, L., Yang, H., Xu, Y., 2016. Ubiquitous production of branched glycerol dialkyl glycerol tetraethers (brGDGTs) in global marine environments: a new source indicator for brGDGTs. *Biogeosciences* 13, 5883–5894. <https://doi.org/10.5194/bg-13-5883-2016>.
- Zanon, M., Davis, B.A.S., Marquer, L., Brewer, S., Kaplan, J.O., 2018. European forest cover during the past 12,000 Years: a palynological reconstruction based on modern analogs and remote sensing. *Front. Plant Sci.* 9, 253. <https://doi.org/10.3389/fpls.2018.00253>.
- Zhang, Y., Renssen, H., Seppä, H., Valdes, P.J., 2018. Holocene temperature trends in the extratropical Northern Hemisphere based on inter-model comparisons. *J. Quat. Sci.* 33, 464–476. <https://doi.org/10.1002/jqs.3027>.
- Zhao, H., Huang, C.C., Wang, H., Liu, W., Qiang, X., Xu, X., Zheng, Z., Hu, Y., Zhou, Q., Zhang, Y., Guo, Y., 2018. Mid-late Holocene temperature and precipitation variations in the quating basin, upper reaches of the yellow river. *Quat. Int.* 490, 74–81. <https://doi.org/10.1016/j.quaint.2018.05.009>.
- Zink, K.-G., Vandergoes, M.J., Mangelsdorf, K., Dieffenbacher-Krall, A.C., Schwark, L., 2010. Application of bacterial glycerol dialkyl glycerol tetraethers (GDGTs) to develop modern and past temperature estimates from New Zealand lakes. *Org. Geochem.* 2009 (41), 1060–1066. <https://doi.org/10.1016/j.orggeochem.2010.03.004>. *Advances in Organic Geochemistry*.
- Zink, K.-G., Vandergoes, M.J., Bauersachs, T., Newnham, R.M., Rees, A.B.H., Schwark, L., 2016. A refined paleotemperature calibration for New Zealand limnic environments using differentiation of branched glycerol dialkyl glycerol tetraether (brGDGT) sources. *J. Quat. Sci.* 31, 823–835. <https://doi.org/10.1002/jqs.2908>.